Chemical Science

ROYAL SOCIETY OF CHEMISTRY

REVIEW

View Article Online
View Journal | View Issue

Cite this: *Chem. Sci.*, 2026, **17**, 96

Ionomers modulate the microenvironment in electrocatalytic CO_2 reduction

Sunhong Ruan,* Gangjun Tang, Zhiming Zhang, Qinghong Zhang,* Ye Wang * and Shunji Xie *

The global shift toward a low-carbon society has accelerated the development of electrocatalytic CO_2 reduction reaction (CO_2RR) technology, which shows great potential in simultaneously addressing environmental pollution and energy crises. In the CO_2RR system, microenvironment modulation can effectively enhance catalytic activity, product selectivity, operational stability, and energy efficiency. The introduction of ionomers into catalyst layers enables precise control of the microenvironment at the catalyst surface through their unique structural properties, significantly improving CO_2RR performance. In this review, we first provide a concise overview of the key components and main influencing factors of the reaction microenvironment and the structures together with the functional mechanisms of commonly used ionomers. We then systematically discuss how various ionomers modulate the microenvironment, including their effects on CO_2 mass transport, stabilization and diffusion of intermediates, ion species and concentrations at the surface (affecting the pH, K^+ distribution and interfacial electric field), surface morphology and hydrophobicity of catalysts, and structures of interfacial water. Finally, we present a comprehensive summary that identifies current practical challenges of ionomer applications from multiple perspectives while proposing feasible solutions and outlining future research directions for this field.

Received 27th September 2025
Accepted 20th November 2025

DOI: 10.1039/d5sc07515g

rsc.li/chemical-science

1. Introduction

Excessive global CO_2 emissions have spurred the rapid development of CO_2 conversion and utilization technologies. The electrocatalytic CO_2 reduction reaction (CO_2RR) has emerged as a promising technology capable of converting CO_2 into high-value-added products, contributing to a low-carbon environment.[1–3] Over the past decade, this field has evolved from prevalent catalyst designs, such as metal catalysts, dual-

State Key Laboratory of Physical Chemistry of Solid Surfaces, Collaborative Innovation Center of Chemistry for Energy Materials, National Engineering Laboratory for Green Chemical Productions of Alcohols, Ethers and Esters, College of Chemistry and Chemical Engineering, Xiamen University, Xiamen 361005, China. E-mail: zhangqh@xmu.edu.cn; wangye@xmu.edu.cn; shunji_xie@xmu.edu.cn

Sunhong Ruan

Sunhong Ruan received his BSc degree from Nanjing University of Aeronautics and Astronautics in 2017 and obtained his PhD degree from Xiamen University in 2024. He is now working in Prof. Ye Wang's group as a post-doctoral fellow at College of Chemistry and Chemical Engineering of Xiamen University (China). His research interest lies in the design of highly efficient electrocatalysts and anion exchange membranes for electrocatalytic CO_2 reduction.

Qinghong Zhang

Qinghong Zhang received her BSc and MSc degrees from Nanjing University in 1989 and 1992 and obtained her PhD degree from Hiroshima University of Japan in 2002. She joined Xiamen University in October 2002 and was promoted to a full professor in 2010. Her research interests include the synthesis and characterizations of novel materials with advanced catalytic properties.

metal catalysts, single-atom catalysts, and diatomic catalysts, to comprehensive optimization of entire system components for efficient and stable operation.[4–14] These advancements include improvements in electrolyzers from single-chamber cells to H-cells, solid oxide cells with perovskite-based fuel electrodes, flow cells and membrane electrode assemblies (MEAs) with gas diffusion electrodes (GDEs),[15–17] development of ion exchange membranes (IEMs) from predominant Nafion membranes to anion exchange membranes and bipolar membranes,[18,19] application of ionomers progressing from a single type ionomer to various ionomer combinations,[20,21] and optimization of system parameters such as electrolysis temperature, pressure and water management.[22–25] Through systematic research and improvements of these key parameters, significant progress has been achieved in performance, including activity, selectivity, energy efficiency, and stability, paving the way for feasible industrial-scale application in the near future. The CO_2RR system usually comprises a cathode, an anode, an ion exchange membrane and multiple interfaces. Chen *et al.* summarized the effect of catalyst surface/interface structures on the CO_2RR process from the perspective of coordination engineering, atomic interface design, surface modification, and hetero-interface construction.[26] The reaction performance is significantly influenced by the microenvironment at these interfaces, making its modulation particularly crucial. Based on extensive research efforts, various approaches have been identified for modulating the microenvironment of the electrode surface: precise design at the catalyst surface through methods like defect engineering, the confinement effect and hydrophobic modification,[27–29] selection of the electrode substrate,[30] electrolyte optimizations,[31] and careful selection of IEMs and ionomers.[18,21,32,33] These modulation strategies about the microenvironment can significantly enhance CO_2RR performances. Currently, comprehensive reviews have systematically summarized these modulation approaches on the microenvironment.[34,35]

During electrode fabrication, organic modifiers are typically introduced as binders to stabilize the catalyst.[32] Common binders include charged ionomers (*e.g.*, Nafion), neutral polymers (*e.g.*, polytetrafluoroethylene (PTFE) and polyamines) and organic small molecules (*e.g.*, pyridine and tetramethylammonium). Compared to neutral modifiers, the uniqueness of ionomers lies in their ability to transport ions (*e.g.*, H^+, OH^-, and K^+) *via* their ionic functional groups, thereby modulating key properties of the catalyst surface microenvironment such as pH, interfacial electric field, and water transport.[20,21,25,36] Ionomers were initially extensively studied and applied in fuel cells and water electrolysis systems.[37–40] Subsequent research demonstrated their direct applicability to the electrocatalytic CO_2RR system, where they play an indispensable role in improving the mass transport of surface species and modulating the microenvironment.[41] Recently, some researchers have reviewed this field. For example, Won *et al.* summarized the roles of binders (including ionomers as one type) in this system, covering their physical benefits for catalysts, chemical interactions, and developmental utilizations.[32] Additionally, Wang *et al.* summarized ionomer designs for the CO_2RR, focusing on strategies to enhance CO_2 mass transport in catalyst layers, modulate local ion concentrations, and control reaction intermediate adsorption.[33] Nonetheless, a comprehensive and in-depth analysis of how ionomers modulate the microenvironment of catalyst surfaces in the CO_2RR system remains lacking, particularly regarding which specific microenvironment is influenced by different ionomers and the underlying mechanisms. Only through a thorough understanding of ionomer-mediated microenvironment modulation can an optimal ionomer selection be achieved and reaction processes/mechanisms be fundamentally understood.

In this review, we first concisely introduce the compositions and roles of the microenvironment in the electrocatalytic CO_2RR, along with commonly used ionomer structures and their mechanistic roles. Although ionomers typically exert

Ye Wang

Ye Wang received his BSc degree from Nanjing University and PhD degree from Tokyo Institute of Technology. He then worked at Tokyo Institute of Technology, Tohoku University and Hiroshima University and was promoted to associate professor at Hiroshima University in 2001. He became a full professor at Xiamen University in August of 2001. He serves as an associate editor of ACS Catalysis and a council member of International Association of Catalysis Societies. The research interest of Prof. Ye Wang's group is catalysis for C1 and sustainable chemistry, including C–H activation and C–C coupling of C1 molecules and C–O/C–C cleavage chemistry for cellulose/lignin valorization.

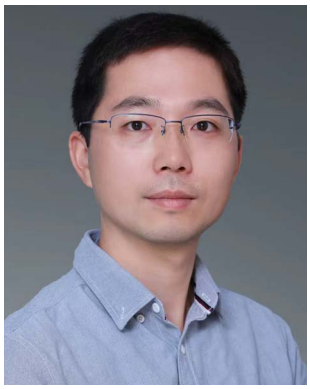

Shunji Xie

Shunji Xie received his BSc and MSc degrees from Hunan University of China in 2008 and 2011 and obtained his PhD degree from Xiamen University in 2014. He then carried out postdoctoral research at the Collaborative Innovation Center of Chemistry for Energy Materials (iChEM). He is currently a full professor in College of Chemistry and Chemical Engineering of Xiamen University. His research interest focuses on photocatalysis and electrocatalysis for C1 and sustainable chemistry, including CO_2 reduction, CH_4 oxidation, biomass conversion and ethylene glycol synthesis.

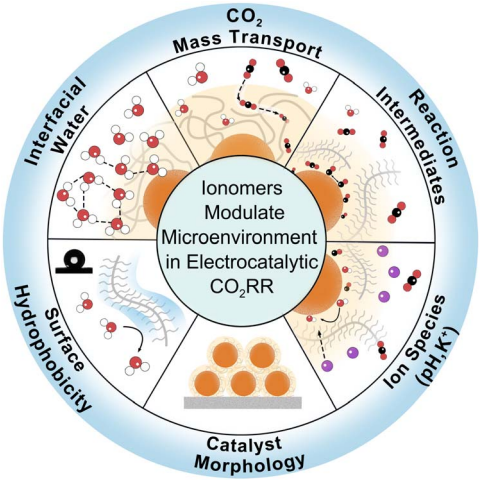

Fig. 1 Ionomers modulate the microenvironment in the electrocatalytic CO_2RR.

multiple functions simultaneously in the reaction system, we find that they can be classified according to a hierarchy of primary and secondary roles, which contributes to clarifying their structure–activity relationship. So, we systematically summarize the ionomer-mediated microenvironment modulation through six key aspects: promoting CO_2 enrichment and mass transport, stabilizing reaction intermediates or facilitating their diffusion, modulating surface ion species and concentrations, stabilizing or adjusting catalyst morphology and state, modulating hydrophobicity of catalyst surfaces, and tuning structures of interfacial water (Fig. 1). Building on these insights, we critically discuss current challenges in ionomer applications for the CO_2RR and propose original perspectives for future ionomer design and implementation strategies.

2. The microenvironment of the electrocatalytic CO_2RR

2.1 Compositions and functions of the microenvironment

The performances of catalysts in the electrocatalytic CO_2RR are determined not only by active sites but also by microenvironment modulation of mass transport, local kinetics, and stability for CO_2 and related species in a heterogeneous reaction.[42,43] In a strict sense, the microenvironment refers to the physicochemical properties of catalysts, while more broadly it encompasses external driving forces in local regions.[44,45] The microenvironment in catalysis involves multiple hierarchical levels: the molecular/atomic-level control of catalysts, involving coordination environments of the active centers and atomic/molecular interactions;[46] the nanoscale/microscale confinement effects, where the confined microenvironment can regulate reactant diffusion and consequently its adsorption/activation on the catalyst surfaces;[47] interfaces and complex surface chemistry involving mass transport, local pH, concentration gradients near active sites, and adsorption behaviours;[35,48,49] physical fields including light, electricity or microwaves.[50] In the electrocatalytic CO_2RR, rational modulation of the microenvironment of electrode surfaces, including catalyst surfaces, electrode architectures, and reactive surface species, can enhance the reaction rate and selectivity, improving the energy efficiency and establishing foundations for industrial implementation.

2.2 Influencing factors of the microenvironment

In the electrocatalytic CO_2RR, the microenvironment primarily refers to the local environment surrounding the reaction interface, which influences both the kinetic and thermodynamic processes of the reaction.[45,51] Here, "local" is typically relative to "bulk", referring to a finite, specific range or scale that differs from the overall, macroscopic, and average conditions of the bulk phase. In the CO_2RR system discussed in this review, the local environment denotes the physicochemical environment at the catalyst surface, with a nanoscale dimension. This local environment primarily differs from the types and concentrations of ions and the water structure in the bulk electrolyte, as well as the bulk CO_2 concentration.[44,45,52,53] In the system, the principal factors influencing the microenvironment include: properties of catalyst surfaces,[54] characteristics of electrode substrates,[30] co-reactants,[55] electrolyte compositions,[31,56] membrane properties,[57–59] and reactor configurations[15,17,60] (Fig. 2a).

A large number of experiments demonstrate that microenvironment modulation can be systematically achieved through: (1) precise engineering of the catalyst surfaces by optimizing atomic/electronic configurations to enhance CO_2 adsorption and activation.[27,28,61,62] For instance, Guan *et al.* summarized strategies for modulating the geometric and electronic structures of the metal centers in the single-atom, diatomic, and triatomic catalysts through the design of substrates, central metal atoms, and coordination environments, thereby influencing the surface microenvironment of catalysts.[61] Besides, the summary by Kolding *et al.* also indicated that in a reaction, designing a tailored microenvironment, particularly by modulating the spatial environment around catalytic active sites, can effectively control the catalytic performance.[62] Apart from these engineering approaches, recently, numerous studies have demonstrated that ionomers can also modulate the microenvironment of catalyst surfaces. Whether the ionomer fully or partially coats the catalyst, it can promote CO_2 mass transport and regulate water transfer, enabling efficient reactions.[20,63] Additionally, ionomers can adjust the ion transport and pH at the catalyst surface and modify the hydrogen-bonded structure of interfacial water to facilitate CO_2 reduction.[21,64] Based on prior studies and our understanding, here, the microenvironment primarily emphasizes the local environment influencing the reaction, spatially encompassing the electric double layer (EDL). The key role of the microenvironment is primarily played by the Helmholtz layer closest to the catalyst surface, with a thickness of approximately 1–2 nm, which includes part of the surfacial ionomer layer. Within the local region, the OH^- and K^+ become enriched, and the structure of interfacial water significantly differs from that of bulk water (Fig. 2b). (2) Strategic design of electrode substrates by incorporating gas diffusion layers to facilitate CO_2 mass transport while concurrently

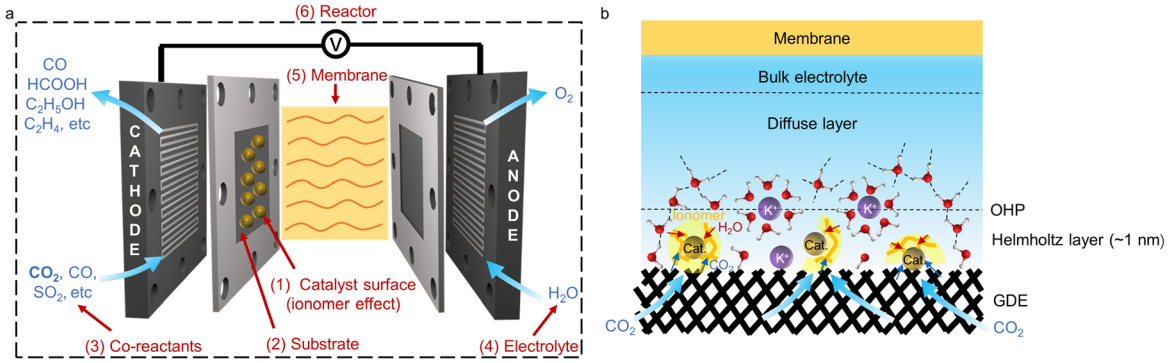

Fig. 2 (a) Influencing factors on the microenvironment in the electrocatalytic CO_2RR. (b) Schematic illustration of the microenvironment at the catalyst surface modulated by ionomers. The terms Cat. and OHP represent the catalyst and Outer Helmholtz Plane, respectively.

improving the electrical conductivity and structural stability.[30,65] (3) Controlled introduction of co-reactants (*e.g.*, CO introduction to selectively promote C_{2+} product formation or coupling with N_2, nitrate species, or organic compounds).[55,66–68] (4) Tailored modifications of electrolyte formulations through the optimization of cation concentrations or incorporation of organic cations/additives to precisely tune reaction selectivity.[31,69] (5) Sophisticated selection and combination of ion exchange membranes to regulate ion/water transport dynamics, establishing optimal interfacial pH conditions and specific ion concentrations at the cathode surface to modulate reaction performances.[18,70–72] (6) Progressive advancement of reactor architectures, evolving from simple H-cells to MEAs, solid-electrolyte devices, and forced convection configurations to enhance both the reaction rate and energy efficiency.[15,17,73,74] To realize the scaled-up implementation of electrocatalytic CO_2 reduction, these critical factors must be holistically designed and synergistically optimized to ensure highly efficient operation of the reaction.

3. Ionomers for the electrocatalytic CO_2RR

3.1 The structures of ionomers

Ionomers typically consist of a polymeric backbone and side chains containing ionic functional groups. The backbone provides mechanical and chemical stability to the whole structure, often exhibiting high hydrophobicity due to the presence of alkyl, aryl, and fluorine-containing functional groups. The ionic side chain primarily controls properties, such as ion exchange capacity (IEC), ionic conductivity, water uptake, and swelling ratio, and is usually the most vulnerable site for degradation.[19,75] Currently, various materials are used to modify catalyst surfaces, including ionomers, neutral organic polymers, covalent organic frameworks (COFs) and so on. Due to their structural difference, these materials exhibit significantly different performance characteristics, requiring careful selection for research purposes. In the field of electrocatalytic CO_2 reduction, Nafion remains the most widely used ionomer for cathodic catalyst modification.[20,57] In recent years, researchers have begun exploring Nafion-like cation ionomers such as Aquivion and perfluorosulfonic acid ionomers (PFSA-L and PFSA-S) (Table 1),[63,76] as well as emerging anion exchange ionomers.[41,77–79] These materials differ in both backbone structures and ionic side chains, resulting in distinct ion transport properties. At 298 K and 1 atm in infinitely dilute water, the ionic mobility of H^+ is 3.623×10^{-7} m^2 s^{-1} V^{-1}, while that of OH^- is 2.064×10^{-7} m^2 s^{-1} V^{-1}.[80] This explains why cation exchange ionomers typically exhibit significantly higher ionic conductivity than anion exchange ionomers. Furthermore, recent studies have shown that anion exchange ionomers generally exhibit inferior mechanical strength and chemical

Table 1 Structures and properties of typical cation exchange ionomers

Names	Structures	Ion groups	IEC (mmol g^{-1})	Ref.
Nafion	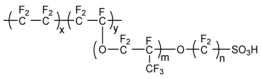	Sulfonate	~0.9	75
Aquivion	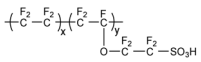	Sulfonate	1.0–1.3	75
PFSA-L	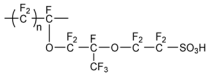	Sulfonate	—	63
PFSA-S	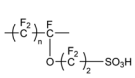	Sulfonate	—	63 and 76

Table 2 Structures and properties of typical anion exchange ionomers

Names	Structures	Ion groups	IEC (mmol g^{-1})	Ref.
Sustainion	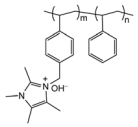	Imidazolium	1.4–1.6	41 and 83
Sustainion XA-9	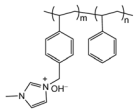	Imidazolium	1.6	84 and 85
1-*n*-alkylimidazolium	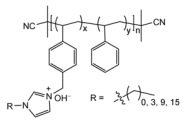	Imidazolium	1.57–2.34	86
Aemion	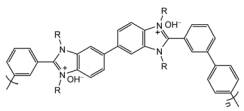	Benzimidazolium	1.4–1.7	36
Fumion	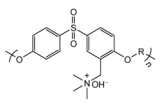	Quaternary ammonium	1.0–1.6	87
QAPEEK	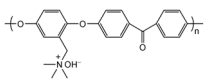	Quaternary ammonium	—	77
Pention		Quaternary ammonium	1.5–2.0	88
Polynorbornene		Quaternary ammonium	—	89
c-PDDA	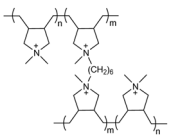	Quaternary ammonium	—	90
PiperION	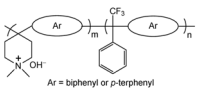	Quaternary ammonium	2.37	78 and 91
QAPPT	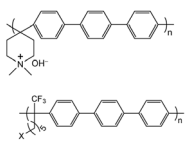	Quaternary ammonium	2.55–2.65	92
*p*TPN-x	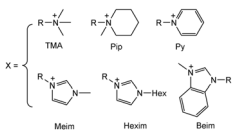	Trimethylammonium/piperidinium/pyridinium/ 1-methyl-imidazolium/1-*n*-hexyl-imidazolium/ 1-methyl-benzimidazolium	—	93
QPC-Z	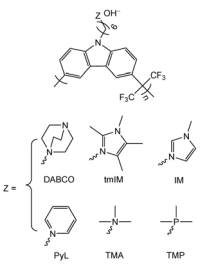	*N*-Methylquinuclidinium/imidazolium/pyridinium/quaternary ammonium/quaternary phosphonium	1.8–2.3	94

stability compared to Nafion-type cation exchange ionomers.[75,81,82] The most common anion exchange ionomer is Sustainion,[41,83] including its derivatives such as Sustainion XA-9,[84,85] as well as imidazolium- and benzimidazolium-functionalized ionomers like 1-*n*-alkylimidazolium and Aemion.[36,86] Recently developed quaternary ammonium-based ionomers are more stable with higher ionic conductivity including Fumion,[87] quaternary ammonium poly(ether ether ketone) (QAPEEK),[77] Pention,[88] polynorbornene,[89] cross-linked poly(diallyldimethylammonium chloride) (c-PDDA),[90] poly(aryl piperidinium)-based anion exchange ionomer (PiperION),[78,91] quaternary ammonium poly(*N*-methyl-piperidine-*co*-*p*-terphenyl) (QAPPT),[92] *para*-terphenyl-trifluoroheptan-2-one-x (organic nitrogenous cations (R_4N^+)) (*p*TPN-x),[93] quaternary ammonium polycarbazole-anion conducting groups (QPC-Z)[94] and so on (Table 2). Studies have demonstrated their crucial roles in the electrocatalytic CO_2RR, such as promoting CO_2 mass transport, enhancing electrode hydrophobicity, and regulating the pH at electrode surfaces.

3.2 Functional mechanisms of ionomers

Ionomers can transport ions through their ion-containing side chain, primarily *via* hydrated ionic domains formed when these functional groups absorb water (Fig. 3a). The mechanisms of ion transport mainly involve two pathways: vehicular transport and Grotthuss hopping.[75,95,96] Vehicular transport includes diffusion driven by concentration gradients and electromigration driven by potential gradients. While these two processes differ in their driving forces, both depend on the ion diffusion coefficients across the ionomer.[97] The ionomer structure and water content significantly influence the diffusion coefficients. Grotthuss hopping refers to forming and breaking covalent bonds from ions (*e.g.*, H^+ and OH^-) with adjacent molecules, propagating through hydrogen-bonded networks of water molecules. Both vehicular transport and hopping mechanisms require the presence of free water within ionomers, specifically in hydrated regions where water molecules have limited interactions with the polymer backbone and side chain. However, hydration must be carefully controlled, as excessive water uptake can cause structural swelling and damage. It is noteworthy that due to the diversity of ion transport mechanisms in ionomers, they typically do not exhibit 100% ion selectivity. For example, Nafion not only transports cations like H^+ and K^+ but also transports anions to a small extent. Nonetheless, Nafion mainly facilitates the transport of H^+, or more precisely, it has the highest transport rate for H^+ among common ions. Because of interactions of ionic charges, ionomers can relatively repel ions of the same charge type (*e.g.*, Nafion, which carries the $-SO_3^-$ ion, repels negatively charged OH^-, while QAPPT, carrying the $-NR_4^+$ ion, repels positively charged H^+). By coordinating ion transport and exclusion, they can modulate the microenvironment at the reaction interface.

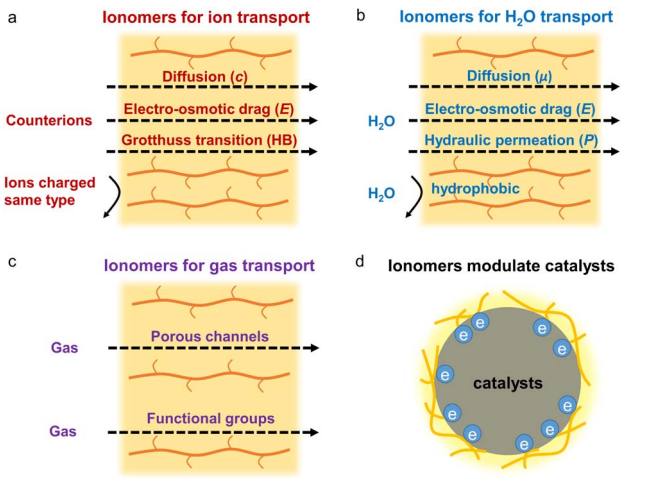

Fig. 3 Functional mechanisms of ionomers transferring (a) ions, (b) H_2O, (c) gas, and (d) modulating catalysts (where *c*, *E*, HB, *μ*, *P*, and *e* represent the concentration, potential, hydrogen bond, chemical potential, pressure, and electron, respectively).

In addition, ionomers can also transport water and gases.[75] Water transport is driven by chemical potential differences across the ionomer (eqn (1)), electroosmotic drag (eqn (2)), or back-convection due to the hydrophilicity/hydrophobicity differences (eqn (3)) (Fig. 3b).[98] Water primarily diffuses through hydrophilic regions formed by ionic groups in the ionomer structure, while hydrophobic groups (*e.g.*, aryl or fluorine functional groups) hinder water permeation. Therefore, water transport in ionomers depends on the synergistic effect of hydrophilic and hydrophobic groups, which can be precisely designed and modulated. Ionomers facilitate gas transport (*e.g.*, H_2, O_2 and CO_2) primarily through their three-dimensional porous channel structures and functional groups (*e.g.*, amine groups) which interact with gas molecules to enable transport (Fig. 3c). Additionally, ionomers can stabilize the morphology and state of catalysts or modulate their electronic structures through interactions between ionic groups and the catalysts, thereby exerting a modulation effect (Fig. 3d).

$$J_{\text{diff}} = \frac{\Delta\mu_{\text{LV}}}{R_{\text{w}} \times A} \tag{1}$$

where R_{w} represents the effective water permeation resistance (a function of the diffusion coefficient D' and ionomer thickness) and $\Delta\mu_{\text{LV}}$ denotes the chemical potential difference for water transport across the iomomer.

$$J_{\text{EOD}} = \frac{j}{F} \times n_{D,\text{avg}} \tag{2}$$

$$J_{\text{HP}} = K\Delta P_{\text{c-a}} \frac{\rho}{M_{\text{H}_2\text{O}}} \tag{3}$$

where K represents the hydraulic permeability and $\Delta P_{\text{c-a}}$ denotes the pressure difference between the cathode and the anode.

4. Ionomers modulate the microenvironment of the electrocatalytic CO_2RR

The unique structure of ionomers and their ability to transport specific ions and water enable them to effectively modulate the

microenvironment when incorporated into catalyst surfaces. The modulations primarily occur through: enhancing CO_2 mass transport, interacting with reaction intermediates, altering surface ion species and concentrations, modifying the morphology and dispersion state of catalysts, improving electrode hydrophobicity, and restructuring interfacial water networks. These effects significantly impact performances and are crucial for rational system designs, catalyst functionalities, and mechanistic understanding of the reaction processes.

4.1 Ionomers enhance CO_2 mass transport

4.1.1 CO_2 transport and enrichment. Beyond conventional roles in ion and water transport, recent studies find that unique chemical and spatial structures of ionomers can also facilitate the transport of gases such as CO_2. In 2020, Sargent's team addressed the limited CO_2 mass transport in conventional H-cells by developing a hybrid catalyst design strategy. Compared to a conventional two-phase interface, the developed hybrid structure (containing the PFSA ionomer) achieves decoupled gas and electrolyte transport at its triple-phase interface (Fig. 4a and b).[20] The PFSA layer coating catalysts extended the gas diffusion distance from submicron to several micrometers through its hydrophobic side-chain regions. This constructed triple-phase interface significantly enhanced CO_2 mass transport, achieving current densities exceeding 1 A cm^{-2} for the CO_2RR. The CO_2 transport pathway begins from the cathodic gas flow channel, passing through the porous hydrophobic carbon paper to reach the side of the carbon paper facing the ion exchange membrane. For catalysts partially coated with PFSA, CO_2 can directly access the catalyst surface. While for catalysts fully coated with PFSA, CO_2 can transport through the hydrophobic structural channels of PFSA to reach the reaction interface formed between the PFSA ionomer and the catalyst. Their modeling studies further introduced a 20 nm-thick interfacial channel between the catalyst and the electrolyte, where the in-plane gas diffusion coefficient (D) differed substantially from the bulk coefficient (D_0). Simulations revealed that the increasing D/D_0 ratio promoted gas transport, extending CO_2 diffusion distances to several micrometers (*versus* <0.5 μm without the channel), dramatically boosting the reaction current density (Fig. 4c and d).

Furthermore, Sinton *et al.* revealed that PFSA exhibited good selectivity in the transport of different gases (Fig. 4e).[99] This is attributed to the solubility of SO_2 *via* strong dipole–dipole interactions with hydrophilic components in PFSA, coupled with its high solubility in water when PFSA absorbs electrolyte (with a solubility of 1.47 mol L^{-1} at 20 °C and 1.0 atm, significantly higher than that of CO_2), which slows down SO_2 transport through PFSA to the catalyst surface. In contrast, CO_2 interacts weakly with PFSA and has low solubility in water, allowing it to transport through the hydrophobic regions of PFSA in the gaseous form. Theoretical simulations indicated that in PFSA, the solubility of SO_2 increased by ~30 times compared to CO_2, while its diffusivity decreased to about one-fifth of that of CO_2

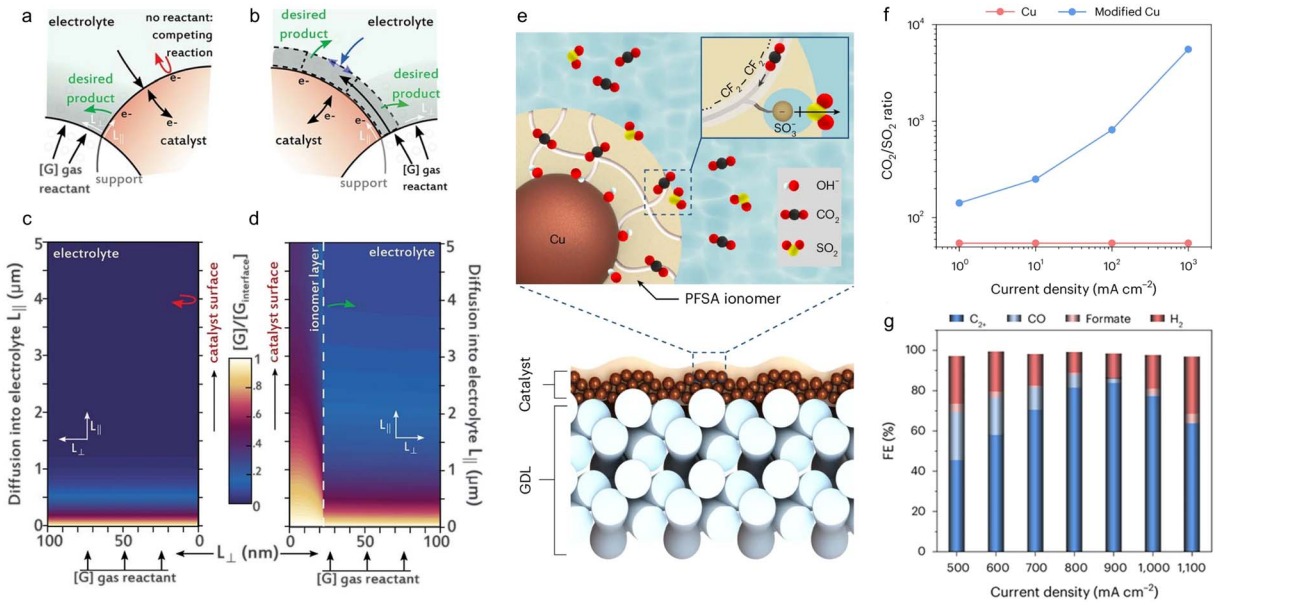

Fig. 4 Ionomers enhance CO_2 mass transport. (a) The volume in which gas reactants, active sites, water, and ions coexist determines the maximum available current for gas electrolysis. Catalyst regions with limited reactant concentration promote by-product reactions. (b) When gas and electrolyte (water and ion source) transport is decoupled, the three-phase reaction interface can be extended so that all electrons participate in the desired electrochemical reaction. Modeled gas reactant availability along the catalyst surface for standard (c) and decoupled (d) gas transport in a 5 M KOH electrolyte. Reproduced with permission from ref. 20. Copyright 2020, the American Association for the Advancement of Science. (e) Schematic of a planar PFSA@Cu/PTFE heterojunction with hydrophilic and hydrophobic characteristics provided by $-SO_3^-$ and $-CF_2$ functionalities for interacting with SO_2 and facilitating CO_2 transport, respectively. (f) Modelled mass flux ratios of CO_2 over SO_2 on the ionomer-modified Cu and bare Cu electrodes during the co-electrolysis of CO_2 and SO_2. (g) Product selectivities from the co-electrolysis of 100% CO_2 and 400 ppm SO_2 on PFSA@Cu/PTFE. Reproduced with permission from ref. 99. Copyright 2024, Springer Nature.

(Fig. 4f). This unique selectivity enabled 790 mA cm^{-2} partial current density for C_{2+} products with 84% selectivity when feeding CO_2 gas containing 400 ppm simulated flue gas impurities by the PFSA@Cu/PTFE heterojunction (Fig. 4g). These studies demonstrate the exceptional capability of ionomers to enhance CO_2 mass transport while enabling selective gas transport for broader industrial applications.

Researchers have also developed other effective ionomers to enhance CO_2 adsorption and mass transport beyond PFSA. Zhuang *et al.* developed a QAPEEK ionomer, which showed a significantly higher selectivity for ethylene production in the electrocatalytic CO_2RR compared to other ionomers (*e.g.*, Sustainion, Fumasep, and PiperION) (Fig. 5a).[77] *In situ* infrared spectroscopy revealed a linear redshift in the asymmetric stretching vibration ($*CO_2$) band center at potentials between 0 and −1.1 V *vs.* the reversible hydrogen electrode (RHE), indicating enhanced interaction between $*CO_2$ and the carbonyl oxygen atom of QAPEEK under electrochemical polarization. This interaction effectively captured CO_2 and stabilized the CO_2 intermediate, facilitating efficient CO_2RR (Fig. 5b and c).

Additionally, Grubbs *et al.* synthesized highly modular three-component copolymers *via* ring-opening metathesis polymerization to modify the Cu electrode, achieving 55% and 77% selectivity for ethylene and C_{2+} products, respectively (Fig. 5d).[100] Combined experimental and molecular dynamics (MD) simulations showed that the improved selectivity was primarily due to the ability of the ionomer to create additional CO_2 diffusion pores, thereby increasing the local CO_2 concentration. Xu *et al.* also developed a novel Cu@poly(ionic liquid) (Cu@PIL) composite, where the ionic liquid contained a tridentate site (one pyridine and two imidazole groups) and two polymerizable alkenyl sites (Fig. 5e).[101] Experimental and theoretical studies demonstrated that isolated ion pairs in the outer PIL layer, particularly the imidazole moieties, enriched CO_2 and directly increased its local concentration. Consequently, both the activity and selectivity for C_{2+} products in the CO_2RR were significantly enhanced. These studies illustrate that various ionomers can effectively enrich, adsorb, and transport CO_2 to improve CO_2RR performance through their CO_2-philic functional groups, spatially ordered channels, and porous architectures.

4.1.2 Modulating CO_2/H_2O transport ratios. The structure of PFSAs can be tailored with variants, including long-side-chain (LSC) and short-side-chain (SSC) PFSAs beyond conventional Nafion. Adjusting the side-chain length alters ionomer properties such as ionic conductivity and hydrophobicity. For instance, Wang *et al.* developed four PFSA ionomers with varying side-chain lengths to optimize CO_2 mass transport (Fig. 6a and b).[63] These ionomers exhibited distinct affinities for CO_2 and H_2O, enabling precise regulation of CO_2/H_2O ratios to establish separate transport channels for each component, improving the microenvironment of catalyst surfaces in MEA. Compared to SSC ionomers, LSC ionomers have higher binding energy with water while lower binding energy with CO_2, indicating enhanced CO_2 transport capability and suppressed water transport (Fig. 6c). Studies further demonstrated that tuning the side-chain length and content of ionomers enhances mass transport networks in catalyst layers. According to the reaction equation, various amounts of water as reactants are required at different current densities, which is essential. This demand can be met through the hydrophilic groups of ionomers to ensure sufficient water supply. When water is abundant, increasing the CO_2/H_2O ratio at the three-phase interface enhances CO_2

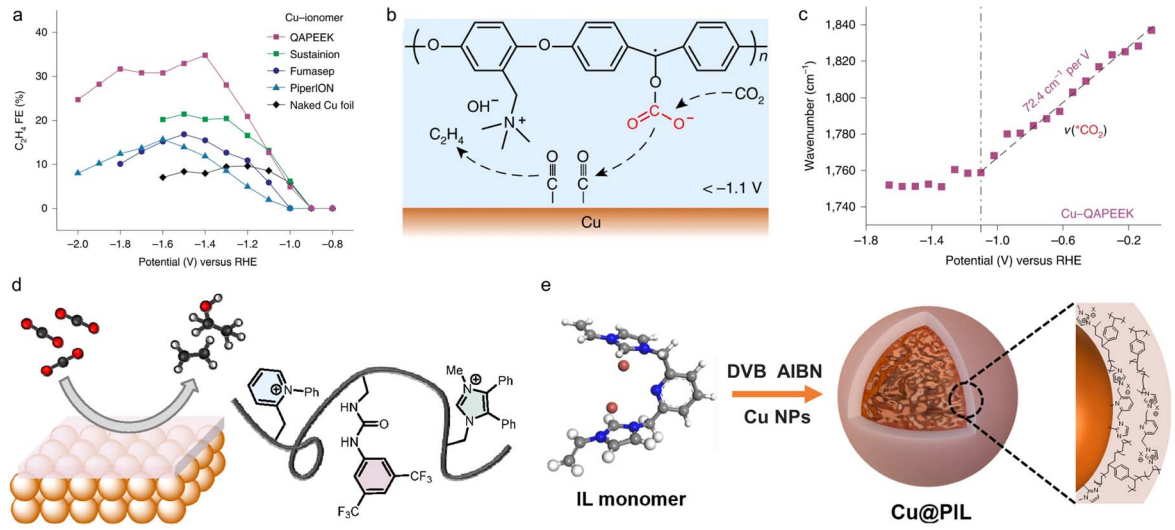

Fig. 5 Ionomers promote CO_2 enrichment on the catalyst surfaces. (a) Different ionomers were tested at a Cu foil electrode with an optimized coating amount for C_2H_4 production. (b) Schematic illustration of the QAPEEK promoting the CO_2RR on Cu. (c) The activated CO_2 ($*CO_2$) signal on Cu-QAPEEK shifted with potential on the naked and QAPEEK-coated Cu electrode surfaces. Reproduced with permission from ref. 77. Copyright 2022, Springer Nature. (d) A tricomponent copolymer modifier on the copper surface enhances the selective electrochemical CO_2RR. Reproduced with permission from ref. 100. Copyright 2021, American Chemical Society. (e) Schematic illustration of the structure of the IL monomer and the preparation of Cu@PIL. Reproduced with permission from ref. 101. Copyright 2021, Elsevier.

coverage on the catalyst surface and promotes CO_2 mass transport. However, when CO_2 coverage reaches saturation, the promotional effect on CO_2 reduction plateaus. Without causing electrode flooding, the amount of water can moderately regulate the catalytic microenvironment and influence the reaction. *In situ* differential electrochemical mass spectrometry (DEMS) identified optimal CO_2 and H_2O transport pathways, while the attenuated total reflection surface-enhanced infrared absorption spectroscopy (ATR-SEIRAS) probed interfacial electrochemical environments, revealing H_2O-deficient and CO_2-deficient zones. It should be noted that they utilized DEMS to detect the ion currents of H_2, C_2H_4, and CO generated during the electrocatalytic CO_2RR. Since the water consumption rates for producing these species differed, the earlier onset potential for H_2 generation observed in the SSC-D72 ionomer system indirectly indicated the presence of more water channels. Conversely, the higher ion currents of C_2H_4 and CO detected in the LSC-D520 ionomer system demonstrated its more developed CO_2 transport channels. Furthermore, MD simulations visualized interfacial CO_2/H_2O distributions. The enhanced CO_2 transport and balanced CO_2/H_2O ratio (high CO_2 and low H_2O concentration) with long-side-chain ionomers achieved 89.4 $\pm$ 0.69% faradaic efficiency for C_{2+} products with a partial current density of 536 $\pm$ 4.1 mA cm^{-2}.

In addition, Takanabe *et al.* found that optimizing Nafion content in Cu catalyst layers significantly improved C_{2+} selectivity, attributed to Nafion's regulation for CO_2 and H_2O diffusion coefficients that enhanced CO_2 transport *versus* bare Cu.[102] Differently, Sinton *et al.* demonstrated that the SSC ionomer (Aquivion) also effectively promoted CO_2 transport by elevating the CO_2/H_2O ratio compared to bare Cu (Fig. 6d and e).[76] The Aquivion-modified Cu catalyst delivered 66% C_2H_4 selectivity with a partial current density of 208 mA cm^{-2}, outperforming the bare Cu (Fig. 6f). These findings underscore the critical role of ionomer-mediated CO_2/H_2O ratio control in increasing the concentration of CO_2 and enhancing performances.

4.2 Ionomers stabilize intermediates or promote intermediate diffusion

The adsorption and stabilization of intermediates can steer reaction selectivity toward a specific product pathway. Ionomers can stabilize CO_2 reduction intermediates or facilitate their diffusion through functional groups, enhancing performance. For instance, by stabilizing *CO to promote C–C coupling for selective C_{2+} production, Zhuang *et al.* prepared six polyaryl ionomers (*p*TPN-X) by grafting different organic cations (TMA, Pip, Py, Meim, Hexim, and Beim) onto ionomers.[93] Electrocatalytic CO_2RR tests revealed that *p*TPN-Beim exhibited the highest C_{2+} selectivity. Cyclic voltammetry and *in situ* IR further demonstrated that $Beim^+$ not only facilitated CO_2 conversion to *CO but also promoted *CO coverage and stability at the electrode surface, increasing the $*CO/H_2O$ ratio and being favorable for subsequent *CO dimerization into C_{2+} products. Additionally, $Beim^+$ significantly enhanced the CO_{LFB}/CO_{HFB} ratio, meaning linearly adsorbed CO dominated over bridge-adsorbed CO, further promoting C–C coupling (Fig. 7a and b). Other researchers have explored tuning intermediate adsorption by varying the side-chain lengths of the ionomer.[86] They synthesized 1-*n*-alkylimidazolium ionomers with different side chain lengths (n = 1, 4, 10, 16) and found that longer side chains suppressed the competing hydrogen evolution reaction (HER) and methane formation. Experimental and computational studies suggested that longer side chains thermodynamically stabilized key intermediates, favoring C_{2+} production.

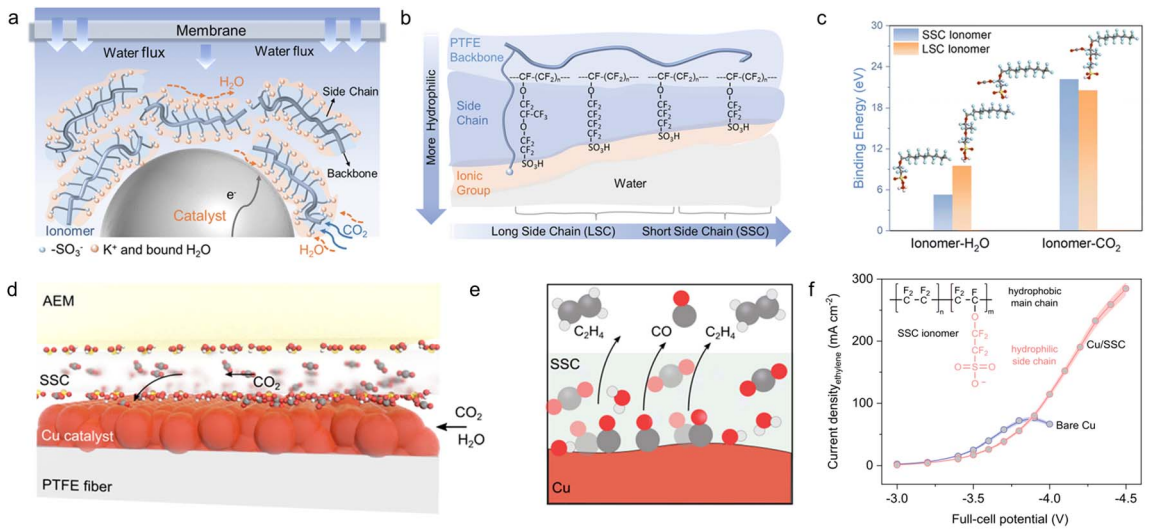

Fig. 6 Ionomers modulate CO_2/H_2O transport ratios. (a) The mass transfer diagram of CO_2 and H_2O channels at the three-phase reaction interface. (b) Chemical structure and hydropathic properties of PFSA ionomers. (c) The density functional theory (DFT) calculation results for the binding energies of ionomer–H_2O and ionomer–CO_2. Reproduced with permission from ref. 63. Copyright 2025, The Royal Society of Chemistry. (d) Enrichment of CO_2 species in the local reaction environment enabled by the SSC ionomer conformably surrounding the Cu surface. (e) Dominancy of the CO_2RR over the HER upon SSC ionomer modification. (f) Ethylene partial current density in a range of applied voltage for bare Cu/PTFE and SSC-modified Cu/PTFE electrodes. Reproduced with permission from ref. 76. Copyright 2020, American Chemical Society.

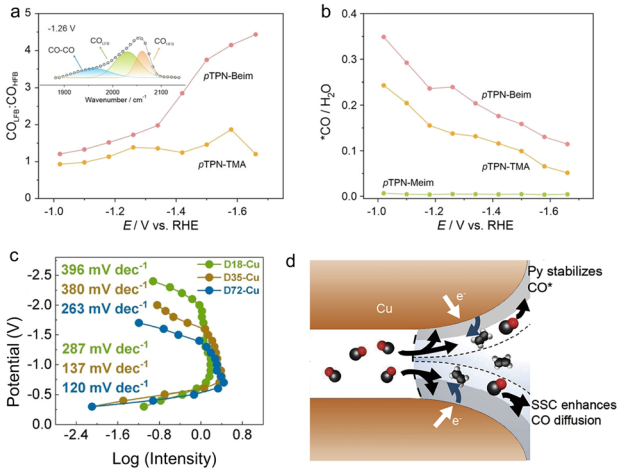

Fig. 7 Ionomers stabilize intermediates or promote intermediate diffusion. (a) Ratio of $*CO_{LFB}$ to $*CO_{HFB}$ band intensities as a function of potential (inset: peak deconvolution of ATR-SEIRAS spectra obtained on Cu/*p*TPN-Beim at −1.26 V *vs.* RHE). (b) Ratio of ν(*CO) to $\nu(H_2O)$ band intensities as a function of applied potential. Reproduced with permission from ref. 93. Copyright 2023, Wiley-VCH. (c) The analysis of the response of the *CO coverage change to potential. Reproduced with permission from ref. 89. Copyright 2023, Wiley-VCH. (d) Introducing additives to improve CO diffusion and stabilize CO* intermediates leads to enhanced C_2H_4 selectivity and activity. Reproduced with permission from ref. 103. Copyright 2021, Elsevier.

In the CO_2RR, if *CO forms and is consumed too quickly, its residence time at the catalyst surface will shorten, reducing C_{2+} yields. To address this problem, Wang *et al.* developed a type of quaternary ammonium-functionalized polynorbornene ionomer (D-X).[89] Its strong hydrophobicity induced an electrokinetic retardation effect, significantly prolonging the *CO residence time on Cu. This unconventional effect was evidenced by increased Tafel slopes and reduced potential sensitivity in *CO coverage (Fig. 7c). In detail, they identified linearly bound *CO (CO_L) by IR and quantified its intensity response with respect to the potential by a data processing method similar to the Tafel analysis. The obtained plots showed slopes of 287, 137, and 120 mV dec^{-1} for CO_L intensity decreasing on the order of D18-Cu, D35-Cu, and D72-Cu, respectively. The descending branch of the CO_L intensity *versus* potential plot had slopes of 396, 380, and 263 mV dec^{-1} for D18-Cu, D35-Cu, and D72-Cu, respectively, indicating that CO hydrogenation is kinetically more favorable at surfaces with weaker hydrophobicity (order of hydrophobicity: D18-Cu > D35-Cu > D72-Cu). The ionomer-modified Cu electrode delivered a C_{2+} partial current density of 223 mA cm^{-2} with 90% selectivity, more than double that of bare Cu.

Beyond stabilization, ionomers can also enhance intermediate diffusion, playing a crucial role in the CO_2–CO–C_{2+} cascade reaction. Sinton *et al.* found that the SSC ionomer ($C_4HF_7O_4S{\cdot}C_2F_4$) promoted the diffusion of *in situ*-generated CO across the electrode surface, boosting C–C coupling for C_2H_4 and other C_{2+} products, with C_2H_4 selectivity reaching 65% (Fig. 7d).[103] These studies demonstrate that ionomers enhance C–C coupling capability by stabilizing the key intermediate or facilitating its diffusion, thereby improving the selectivity for C_{2+} products. They also highlight the critical role of *in situ* characterization techniques, such as IR spectroscopy, in elucidating how ionomer structures regulate the special intermediate.

4.3 Ionomers modulate ion species and concentrations at the catalyst surfaces

Cation exchange ionomers with anionic groups like SO_3^- and anion exchange ionomers with cationic groups like NR_4^+ selectively transport cations (*e.g.*, H^+) and anions (*e.g.*, OH^-), respectively. This selective transport directly influences the local pH, electric field strength, and K^+ concentration at the catalyst surface. They are critical factors for reaction performances. Therefore, designing and selecting an appropriate ionomer can effectively promote target product formation in the electrocatalytic CO_2RR within a specific system.

4.3.1 Modulating pH. Studies have demonstrated that locally alkaline environments could enhance the selectivity of the electrocatalytic CO_2RR.[69] Therefore, achieving high local pH through ionomer modulation is critical for improving this reaction. The type and structure of ionomers determine the species and quantity of ions transported, enabling precise modulation of reaction interfaces to influence performances. The local pH here reflects the ion species (H^+ or OH^-) closest to the catalyst surface, and the microenvironment is primarily influenced by the types and concentrations of ions within the EDL. The experimentally measured pH depends critically on the detection depth of the characterization technique. For instance, with *in situ* surface-enhanced Raman and infrared spectroscopy, the effective detection depth is ~200 nm from the electrode surface, while the dominant signal contribution originates from the ionic species within several nanometers.[104,105] When an ionomer coats the catalyst surface, the pH mainly reflects the relevant ion concentration at the interface between them. Spatially, the measured partial ion concentration can extend into the ionomer layer.

Xie *et al.* employed an anion exchange ionomer (AEI) Pention D-18 to modulate the local pH at catalyst surfaces.[88] Through *in situ* Raman spectroscopy, HCO_3^- and CO_3^{2-} signals were probed at the catalyst surface, and their ratio was used to calculate the surface pH (Fig. 8a and b). The results showed that while the pH at proton exchange ionomer (PEI)-modified Cu catalysts was stabilized at ~10 with increasing current, AEI-modified Cu achieved a progressively higher pH (Fig. 8c), favoring C_{2+} production with 85.1% selectivity at 800 mA cm^{-2}. Theoretical calculations revealed that elevated pH reduced the energy barrier for the rate-limiting OCCO* hydrogenation to OCCOH*. Besides, there were other researchers tuning the interfacial microenvironment at Ag catalysts by varying alkyl chain lengths in imidazolium ionomers.[106] They found these ionomers could maintain alkaline conditions by restricting interfacial water/proton transport, achieving 90.1% CO selectivity. These studies demonstrate that ionomer-induced pH elevation effectively enhances CO_2RR selectivity.

To prevent salt accumulation at the cathode in the CO_2RR, recent scholars explored replacing the alkali-containing anolyte

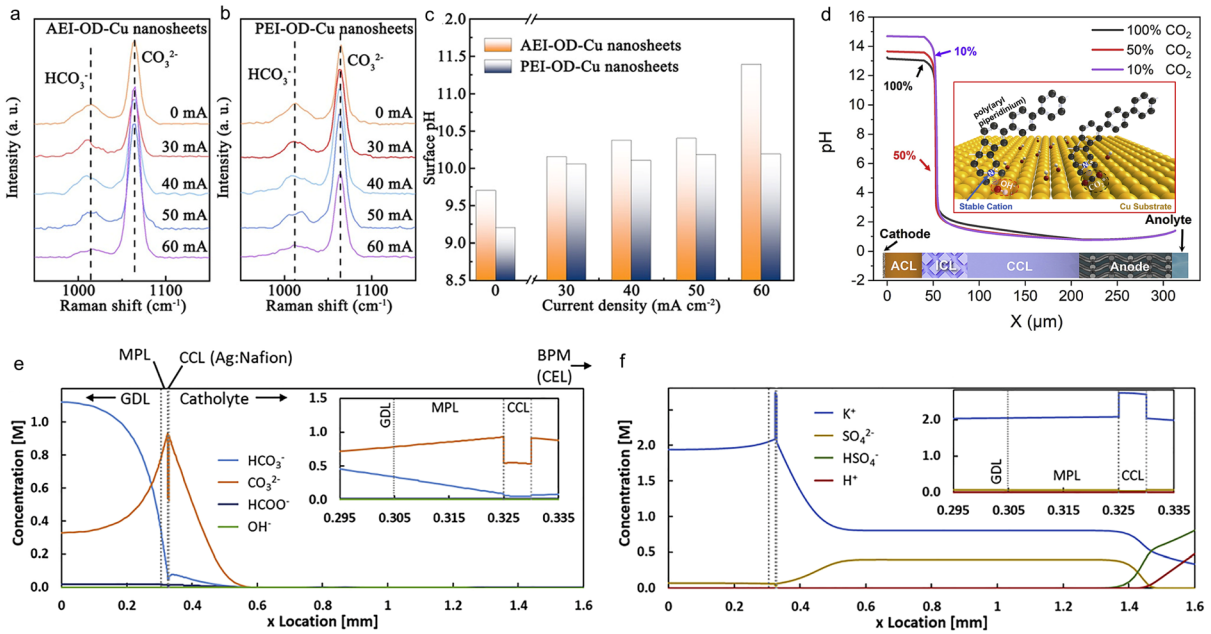

Fig. 8 Single ionomer modification modulates interfacial pH in the electrocatalytic CO_2RR. (a) *In situ* Raman spectra obtained from AEI-modified Cu nanosheets (AEI-OD-Cu) and (b) PEI-modified Cu nanosheets (PEI-OD-Cu). (c) pH values calculated from *in situ* Raman spectra collected at the open-circuit potential and 60 mA cm^{-2}, measured in a flow cell with KOH electrolyte. Reproduced with permission from ref. 88. Copyright 2022, American Chemical Society. (d) COMSOL simulation showed the pH distribution at different dissolved CO_2 contents (100% is the ambient CO_2 solubility limit). Reproduced with permission from ref. 78. Copyright 2022, Elsevier. COMSOL-simulated 1D cross-sections of solution species concentrations at 500 mA cm^{-2} using 0.4 M K_2SO_4 (pH = 7) as the electrolyte with Ag/Nafion electrodes: (e) Concentrations of HCO_3^-, CO_3^{2-}, $HCOO^-$, and OH^-. (f) Concentrations of K^+, SO_4^{2-}, HSO_4^-, and H^+ (insets show magnified views within the catalyst layer). Reproduced with permission from ref. 107. Copyright 2022, Elsevier.

with pure water or pure acid solution. However, this often causes severe pH drop due to missing alkali cations. Sinton *et al.* addressed this by modifying Cu with an anion exchange ionomer PiperION, maintaining >80% selectivity at 40–240 mA cm^{-2} while hypothesizing an alkaline cathode surface.[78] COMSOL simulations confirmed a high local pH near the cathode surface regardless of CO_2 concentrations (100%, 50%, or 10%) (Fig. 8d), showing that cationic groups of PiperION could effectively confine OH^- while blocking H^+ migration, mimicking alkali cation effects. Additionally, through 2D multiphysics modeling, 1D species distributions at the surface of ionomer-containing catalyst layers were revealed.[107] Simulations indicated the SO_3^- group of Nafion induced Donnan exclusion of CO_3^{2-}/HCO_3^-, sustaining high CO_3^{2-} concentrations after HCO_3^- conversion to elevate the pH (Fig. 8e). The cathode surface exhibited markedly increased K^+ and reduced H^+ concentrations (Fig. 8f), demonstrating how ionomers optimized CO_2RR selectivity *via* controlling the pH. Evidently, significant advances in *operando* characterization techniques and simulations have enabled precise interfacial pH modulation through ionomers.

Interestingly, Bell *et al.* made the first attempt to use bilayer ionomers to modulate the microenvironment at the electrode surface, including the pH and CO_2/H_2O ratios.[21] They ingeniously designed comparisons of catalytic performance and surface pH among bare Cu surfaces, Nafion-modified Cu surfaces, Sustainion-modified Cu surfaces, Nafion (inner layer)/Sustainion (outer layer)-modified Cu surfaces, and Nafion (outer layer)/Sustainion (inner layer)-modified Cu surfaces (Fig. 9a and b). The study found the two ionomers played distinct roles: Sustainion increases CO_2 solubility, while Nafion enhanced the local pH by trapping OH^- and blocking HCO_3^- from entering the reaction interface. This led to an optimal configuration, Naf850/Sus/Cu, where the Sustainion inner layer near the Cu surface increased the CO_2 concentration, while the Nafion outer layer trapped *in situ*-generated OH^- from the catalyst and blocked HCO_3^- to elevate the interfacial pH (Fig. 9c), synergistically achieving the highest CO_2RR selectivity (90% C_{2+} products, only 4% HER). In contrast, the Sus/Naf850/Cu configuration significantly reduced the CO_2/H_2O ratio at the catalyst surface and exhibited poor OH^- trapping, leading to a notable pH decrease and exacerbated the HER (Fig. 9d). Fig. 9e clearly demonstrates that AEI can increase the CO_2/H_2O ratio (*i.e.*, CO_2 concentration), while the combination of AEI (inner layer)/cation exchange ionomer (CEI outer layer) further elevates local pH, thereby synergistically enhancing C_{2+} product selectivity. This study about the sophisticated combination of CEI and AEI provides invaluable guidance for the synergistic use of different ionomers.

Besides, Ngene *et al.* conducted similar studies on bilayer ionomer-modified electrodes and drew consistent conclusions: Sustainion monolayer modification aggravated the HER.[108] Nafion, whether as a monolayer or as an outer layer over Sustainion, promoted C_{2+} product formation. There were

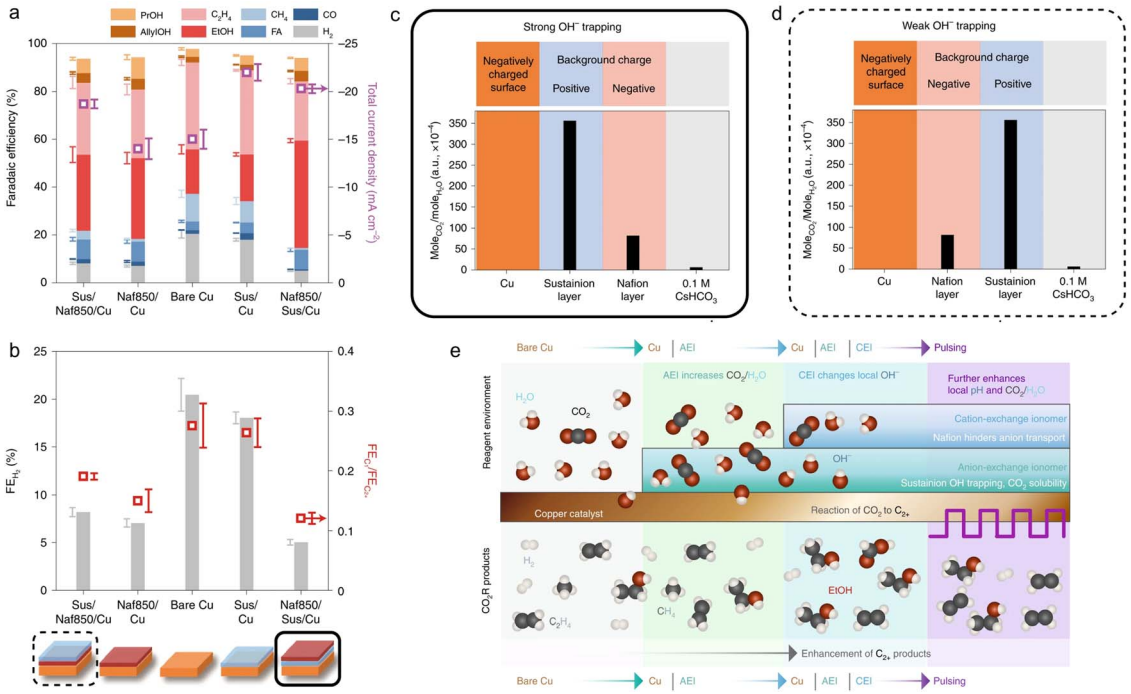

Fig. 9 Bilayer ionomers modulate the interfacial pH in the electrocatalytic CO_2RR. (a) CO_2RR performance of stacked-ionomer-modified Cu in 0.1 M $CsHCO_3$ electrolyte at −1.15 V *vs.* RHE. (b) Product distribution trends for stacked-ionomer-modified Cu catalysts. Schematic illustrations of Naf850/Sus/Cu (c) and Sus/Naf850/Cu (d) configurations, showing CO_2/H_2O ratios and space-charge distributions. (e) Mechanism of the ionomer-enhanced CO_2RR: an AEI layer on Cu increases the CO_2/H_2O ratio, while a subsequent CEI outer layer creates a bilayer microenvironment that modulates the local OH^- concentration. Reproduced with permission from ref. 21. Copyright 2021, Springer Nature.

additional findings, including Nafion mitigated salt deposition and agglomeration of the Cu catalyst, while Sustainion shifted product selectivity from ethylene to ethanol to some extent. These results demonstrate that the ordered combination of cationic and anionic ionomer layers simultaneously improves CO_2 adsorption on the catalyst surface and elevates the interfacial pH, which is very important for enhancing reaction selectivity.

4.3.2 Enrichment of alkali metal cations. Recent studies have shown that alkali metal cations play crucial roles in the electrocatalytic CO_2RR, such as increasing pH at catalyst surfaces, stabilizing intermediates, and modulating interfacial electric fields.[84,109–114] Among them, Koper *et al.* made significant contributions. Through rigorous experiments, characterization studies, and DFT calculations, they demonstrated that the CO_2RR did not occur on Cu, Au, or Ag electrodes in the absence of metal cations in solution. The dominant role of alkali metal cations is to stabilize the CO_2 intermediate through short-range electrostatic interactions after partial desolvation.[114] Their work proved that positively charged species in the electrolyte were the main factor stabilizing key reaction intermediates. Clearly, surface enrichment of alkali metal cations like K^+ is essential for reaction performances without causing salt precipitation. To enrich K^+ on the catalyst surface, Agapie *et al.* synthesized a series of polystyrene-based ionomers (Fig. 10a).[115] By adjusting the ratio of different blocks in the ionomers, they effectively modulated the K^+ content. When these ionomers were used to modify Cu electrodes, they regulated the local K^+ concentration at the electrode surface. Studies showed that the partial current density of C_{2+} products increased with higher K^+ content in the ionomers (Fig. 10b). However, when K^+ was substituted by organic cations like Me_4N^+, the selectivity dropped to the level of bare Cu, highlighting the critical role of K^+ in enhancing the product selectivity of CO_2 reduction. Further MD simulations revealed that CO_2 diffusivity increased with the higher K^+ concentration, indicating that these ionomers effectively promoted CO_2 mass transport.

Moreover, researchers have recently discovered that COFs, owing to their porous structures, can be specifically designed to enrich both CO_2 and K^+. The COF is a type of material distinct from an ionomer, because the COF is a long-range ordered, porous crystalline material formed by strong covalent bonds linking structural units, while the ionomer is a long-range disordered amorphous/semi-crystalline material containing polymer chains with ionic groups. However, through functional designs, some COFs can exhibit ionomer-like characteristics, such as introducing ionic groups into COFs to enable ion transport like ionomers, thereby becoming ionic polymers. For instance, Wang *et al.* developed a two-dimensional sulfonated COF nanosheet (COF-NS) ionomer (NUS9) (Fig. 10c).[116] When used to modify a Cu catalyst, it increased methane selectivity in the electrocatalytic CO_2RR over 60% under both acidic (pH = 2) and alkaline (pH = 14) conditions. Through XPS depth profiling analysis and K^+ retention experiments, they confirmed that the pore walls of NUS9 contained high-density sulfonic and

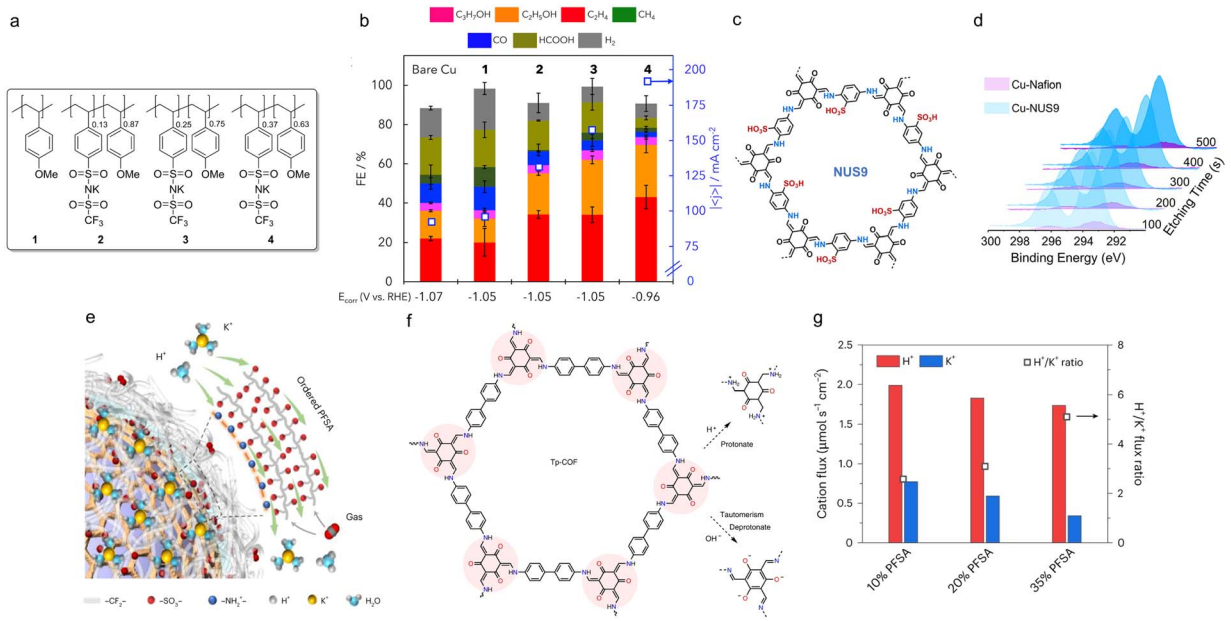

Fig. 10 Ionomers promote K^+ enrichment at surfaces in the electrocatalytic CO_2RR. (a) Structures of a series of synthesized ionomers. (b) Catalytic performances of Cu/PTFE modified with ionomers 1–4 in 1 M $KHCO_3$ electrolyte. Reproduced with permission from ref. 115. Copyright 2024, Elsevier. (c) Chemical structure of NUS-9. (d) X-ray photoelectron spectroscopy (XPS) depth profiles of K in Cu–Nafion and Cu–NUS9 electrodes after CO_2 reduction. Reproduced with permission from ref. 116. Copyright 2024, American Chemical Society. (e) Schematic of functionalized COF particles modulating the ionomer structure and local ion/gas transport. (f) Structure of amphoteric Tp-COF and its sensitivity to the surrounding acidity. (g) Apparent cation fluxes across different COF : PFSA composite layers and the corresponding H^+/K^+ flux ratios at 200 mA cm^{-2}. Reproduced with permission from ref. 117. Copyright 2023, Springer Nature.

carbonyl groups that enriched K^+ (Fig. 10d). Here, K^+ retention experiments were conducted under applied potential throughout the test, and results closely reflected surface-adsorbed K^+ in the EDL. In contrast, XPS depth profiling analysis was performed after cleaning the catalyst surface, detecting K^+ strongly interacting with the NUS9. Comparing the catalytic performances of Nafion-modified and NUS9-modified Cu in electrolytes with varying K^+ concentrations, they found that reducing the K^+ concentration decreased the extent of *CO conversion to multi-electron reduction products at Nafion-modified Cu, while NUS9-modified Cu showed minimal changes. This indicated that NUS9 could maintain a high local K^+ concentration even at low bulk cation levels. Similarly, Sargent *et al.* combined another COF with the PFSA ionomer to create a heterogeneous catalyst coating (Fig. 10e).[117] The study revealed that Tp-COF, containing imine and carbonyl groups, modulated PFSA dispersion and molecular configuration of PFSA, creating uniformly distributed cationic and hydrophilic–hydrophobic nanochannels. This formed an efficient proton flux-limiting overlayer (Fig. 10f). The COF further enriched cations on the catalyst surface (Fig. 10g), improving the reaction microenvironment. As a result, 75% C_{2+} product selectivity at 200 mA cm^{-2} was achieved for the electrocatalytic CO_2RR even under strongly acidic conditions. These findings collectively demonstrate that it is an efficient way to enrich K^+ through ionomers in enhancing CO_2RR performances.

4.3.3 Modulating the intensity of the interfacial electric field. In an acidic electrolyte, alkali metal cations can modify interfacial electric fields, buffer local pH and regulate interfacial water networks to promote the electrocatalytic CO_2RR.[52,53,118] However, the accumulation of alkali metal cations ultimately leads to salt deposition on cathodic catalyst surfaces and electrode failure. Therefore, researchers have sought to use ionomers as substitutes for alkali metal cations to modulate the interfacial electric field. Sinton *et al.* employed a modified Poisson–Boltzmann model in COMSOL to predict the interfacial electric fields generated by K^+ and immobilized cationic groups (CGs) (Fig. 11a–c).[36] In the Gouy–Chapman–Stern (GCS) model, the ionomer was assumed to be uniformly distributed at the catalyst surface, which may lead to some deviations from actual conditions. Nonetheless, calculations based on the GCS model could still provide some valid predictions and guidance. In the model, the OHP was defined by the plane formed by cations carried by ionomer layers closest to the catalyst surface. MD simulations revealed that CGs could generate an interfacial electric field of the same order of magnitude as K^+, with the OHP on the Cu surface coated with CGs being ~6.4 Å (Fig. 11d). Simulations showed that the electric field induced by K^+ and CGs could stabilize negatively charged CO_2, promoting CO_2 adsorption and activation. In contrast, the effect of H^+ on the electric field was negligible compared to K^+ and CGs. On the Cu surface, CG modification resulted in the lowest water density across different potentials, indicating the H_3O^+-blocking effect while simultaneously enhancing the local CO_2 concentration under an applied potential. Based on these simulations, they modified Cu catalysts with the moderate concentration of the

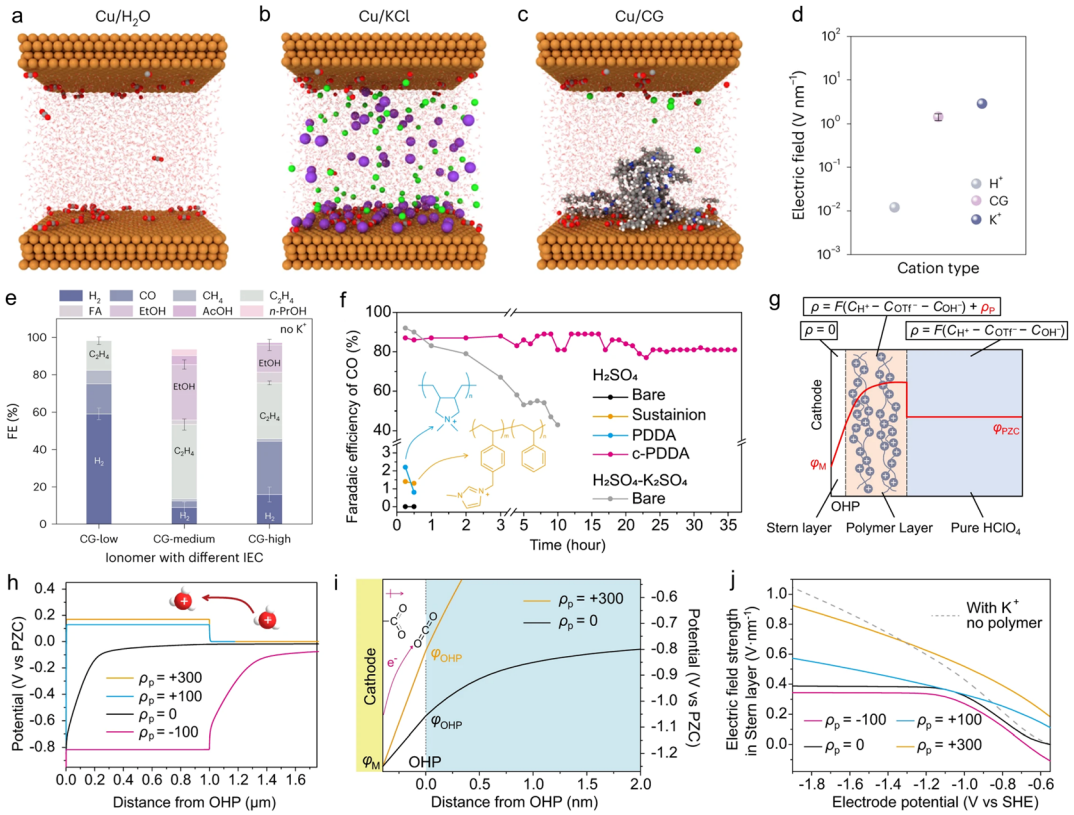

Fig. 11 Ionomers modulate the interfacial electric field in the electrocatalytic CO_2RR. MD-simulated atomic configurations of (a) Cu/H_2O, (b) Cu/KCl, and (c) Cu/CG systems at the end of NVE simulations ($\Delta U = 2.5$ V). (d) Comparison of electric fields generated by H^+, K^+, and CG in the OHP. (e) Catalytic selectivity of Cu modified with CG-low, CG-medium, and CG-high in 0.2 M H_2SO_4 at 100 mA cm^{-2}. Reproduced with permission from ref. 36. Copyright 2023, Springer Nature. (f) FE for CO production on different ionomer-modified Ag catalysts at 200 mA cm^{-2} (electrolyte: 0.1 M H_2SO_4; bare Ag nanoparticle system used 0.4 M K_2SO_4 as an additive). (g) Simulation model: ρ denotes the total charge density; ρ_p represents the charge density carried by the ionomer layer. (h) Potential profiles on Ag electrodes covered by ionomer layers with different ρ_p values (unit: C cm^{-3}) in 10 mM HOTf at −1.8 V *vs.* SHE. (i) Potential profiles on Ag electrodes coated wth ρ_p = 300C cm^{-3} and $\rho_p = 0$ ionomer layers. (j) E_{Stern} *versus* electrode potential. Solid curves: Ag electrodes with different ρ_p ionomer layers (unit: C cm^{-3}) in 10 mM HOTf. Gray dashed curve: the bare Ag electrode in 10 mM HOTf + 40 mM KOTf. Reproduced with permission from ref. 90. Copyright 2023, Springer Nature.

cationic ionomer (Aemion$^+$), achieving 80% C_{2+} product selectivity at 100 mA cm^{-2} under acidic conditions (Fig. 11e).

Gu *et al.* conducted a more in-depth study on ionomer-mediated interfacial field modulation.[90] Previous research showed that bicarbonate formation at the cathode surface was unavoidable even in an acidic electrolyte. However, the system requires cation enrichment in the OHP to alter the electric double-layer field distribution, thereby suppressing H^+ migration through shielding of the cathode field. Additionally, cations stabilize polar intermediates in CO_2 reduction by enhancing the electric field of the Stern layer. Theoretically, cationic ionomers can replace alkali metal cations. Gu *et al.* compared various polyelectrolytes and found that PDDA had the highest cationic density (6.19 mmol g^{-1}), approximately three times that of Sustainion XA-9 (2.06 mmol g^{-1}).[90] When used in the acidic CO_2RR, PDDA performed poorly due to its high solubility in the electrolyte. However, cross-linked PDDA (c-PDDA) delivered near 90% CO selectivity at 200 mA cm^{-2} with stable operation exceeding 35 hours (Fig. 11f). Subsequent GMPNP simulations showed that ionomers significantly altered the charge density distribution in the OHP (Fig. 11g). The simulated potential distribution revealed that the positively charged ionomer layer shielded H^+ migration from the bulk electrolyte to the cathode, with the shielding efficiency increasing with the ionomer charge density (Fig. 11h). Ionomers also affected the field strength of Stern layer (E_{Stern}). Adsorbed CO_2 (*CO_2) possesses a solution-oriented dipole moment, which can be stabilized by E_{Stern} (Fig. 11i). Thus, regardless of the mechanisms of CO_2 reduction, enhancing the E_{Stern} accelerated the reaction. Simulations indicated that ionomers with +300C cm^{-3} charge density produced a higher E_{Stern}, demonstrating that cationic ionomer layers promoted CO_2 reduction at electrode surfaces. Comparisons of E_{Stern} on Ag electrodes coated with different ionomers showed that neutral or anion ionomers could not continuously accelerate CO_2 reduction with increasing overpotential, as E_{Stern} plateaued after initial enhancement. In contrast, cationic ionomers enabled E_{Stern} to increase steadily with more negative potential, with the +300C cm^{-3} ionomer matching the promotional effect of K^+ (Fig. 11j). It is clear that the enhanced interfacial electric field induced by ionomers improved the performance of the electrocatalytic CO_2RR. It is noteworthy that compared to K^+ (0.04 mol L^{-1}) in

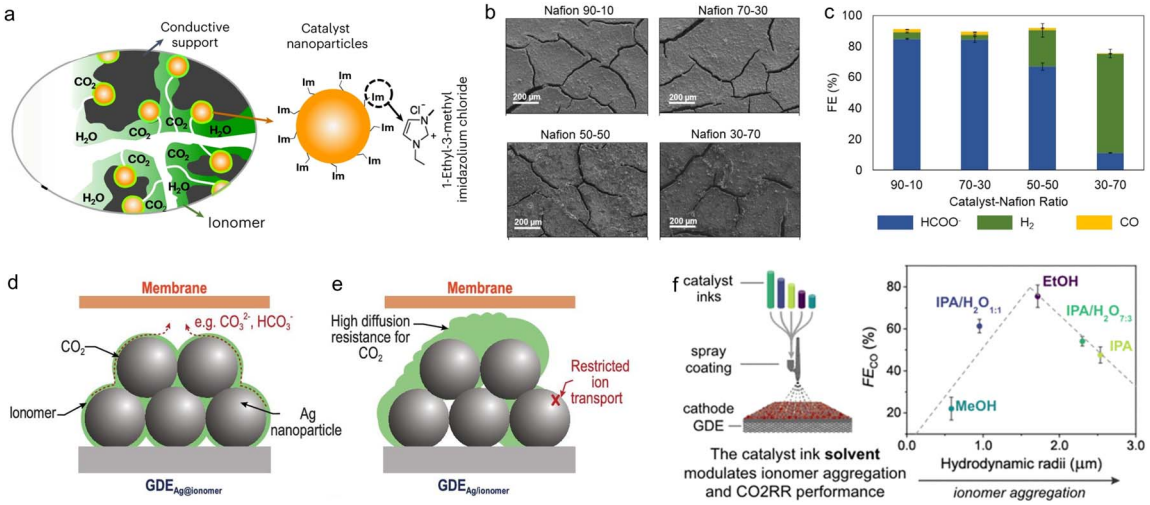

Fig. 12 Ionomers stabilize or modulate catalyst surfaces. (a) Schematic of the catalyst microenvironment composed of Mo_3P nanoparticles covered by an Im layer coated with an anion exchange ionomer and deposited on a conductive carbon support. Reproduced with permission from ref. 85. Copyright 2023, Springer Nature. (b) Scanning electron microscopy images and water contact angle measurements of GDEs prepared with varying catalyst/Nafion ratios. (c) Product selectivity at different catalyst–Nafion ratios. Reproduced with permission from ref. 121. Copyright 2025, American Chemical Society. Schematic of GDE fabrication *via* (d) Ag@ionomer and (e) Ag/ionomer. Reproduced with permission from ref. 122. Copyright 2024, Oxford University Press. (f) Correlation between dispersion solvents, ionomer aggregation, and CO FE. Reproduced with permission from ref. 123. Copyright 2021, American Chemical Society.

the study, the cation density of the ionomer PDDA is relatively low. Moreover, since cations from PDDA are fixed to the polymer chains, their mobility is often restricted, which may result in an electric field generated by PDDA being significantly weaker than that generated by K^+. However, simulations showed comparable interfacial electric fields by them, likely due to the behaviour differences in how these cations form the EDL. Nonetheless, many ionomers can achieve catalytic performances in pure acid or pure water similar to those in the system containing certain concentrations of alkali metal cations.[64,77,90,92,93,119] Besides, in the same way, the interfacial electric field can be modulated by the QAPPT ionomer.[120] In acidic MEA, addition of QAPPT shielded the cathode field, inhibiting H^+ and K^+ cross-membrane diffusion. This improved CO selectivity, achieving 95.6% FE at 100 mA cm^{-2}.

4.4 Ionomers stabilize or modulate catalyst morphology and state

The stability of catalyst surfaces is crucial for the steady operation of the electrocatalytic CO_2RR. When ionomers are introduced onto catalyst surfaces, their high stability often prevents catalyst deactivation. For instance, Asadi *et al.* found that the ionomer Sustainion XA-9 stabilized imidazole (Im)-functionalized Mo_3P nanoparticles, enabling stable operation at nearly 400 mA cm^{-2} for 100 h while maintaining ~90% propane selectivity (Fig. 12a).[85] Post-analysis revealed that Sustainion XA-9 primarily preserved the structural integrity of the organic Im modifiers, preventing their decomposition. Beyond stabilizing catalyst surfaces, ionomers can also directly influence catalyst dispersion. For instance, researchers prepared four different electrodes by adjusting the catalyst-to-Nafion ratio and observing that Nafion significantly altered catalyst dispersion, modifying surface morphology (Fig. 12b).[121] Their results indicated that the Nafion content should not exceed 30%, because a higher proportion would exacerbate the HER (Fig. 12c). Similarly, Sustainion was found to suppress the HER regardless of loading amounts. However, exceeding 30% Sustainion would block CO_2 transport, ultimately reducing the product selectivity.

Furthermore, researchers innovatively proposed a pre-confinement ionomer (PiperION) during catalyst synthesis, ensuring uniform outer-layer encapsulation.[122] Compared to simple mixing (Ag/ionomer), the pre-confinement method yielded Ag@ionomer with more homogeneous distribution, enhancing CO_2 mass transport (Fig. 12d and e). Furthermore, Berlinguette *et al.* discovered that ink solvents influenced the ionomer dispersion, affecting the microstructure of the catalyst layers on GDE and performance.[123] Using methanol, ethanol, isopropanol, and isopropanol/water mixtures, they found ethanol promoted moderate ionomer aggregation, achieving the highest catalytic performance (Fig. 12f). There was another study that examined spray-coating techniques for ionomer application.[124] Results showed that Nafion content critically impacted the dispersion uniformity of catalysts on GDEs, with the automated spraying outperforming manual methods, highlighting the importance of an optimized deposition process. Collectively, these findings demonstrate that rational selection of ionomer types, loading amounts, and adding methods will influence catalyst stability and surface morphology and state, ultimately regulating reaction performances.

4.5 Ionomers modulate the hydrophobicity of catalyst surfaces

In the electrocatalytic CO_2RR, water directly contacts the catalyst surface as a reactant, often leading to surface flooding

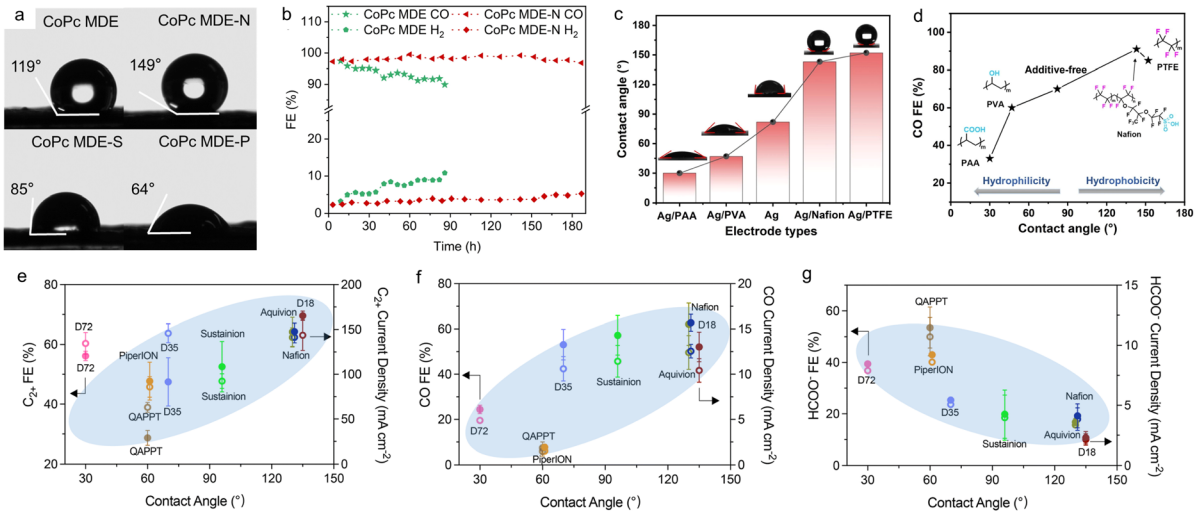

Fig. 13 Ionomers modify the hydrophobicity of electrodes and catalyst surfaces. (a) Water contact angles of CoPc-MDE systems. (b) Stability tests of the CoPc-MDE electrode at 100 mA cm^{-2}. Reproduced with permission from ref. 91. Copyright 2024, The Royal Society of Chemistry. (c) Contact angles of the bare Ag electrode *versus* the polymer/ionomer-modified Ag electrode. (d) Correlation between the CO faradaic efficiency and the contact angle at 200 mA cm^{-2}. Reproduced with permission from ref. 125. Copyright 2025, Elsevier. Selectivity correlations with contact angles for: (e) C_{2+} products at −4.3 V ± 0.1 V, (f) CO at −3 V ± 0.2 V, and (g) formate at −3 V ± 0.2 V at the Cu electrode coated with different ionomers. Light blue shadings are used to represent the correlation trend. Reproduced with permission from ref. 126. Copyright 2024, The Royal Society of Chemistry.

under high current density or prolonged operation. This makes maintaining the hydrophobicity of the catalyst surface critically important. In high-efficiency flow cells and MEA, the triple-phase interface is essential for reaction selectivity. If the electrode hydrophobicity is destroyed, leading to flooding, the reaction irreversibly shifts toward the competing HER. Thus, significant efforts have been made to design and improve the hydrophobicity of electrode surfaces. Ionomers, containing the hydrophobic backbone or functional group, can effectively prevent electrode flooding. For example, Gao *et al.* used three ionomers (Nafion, Sustainion, and PiperION) to modify Ag nanoparticles and molecularly dispersed cobalt phthalocyanine (CoPc MDE).[91] They found these ionomers had minimal impact on the hydrophobicity of the Ag electrode but significantly affected CoPc MDE (Fig. 13a). Nafion notably enhanced the hydrophobicity of CoPc MDE, enabling stable operation for 180 h at 100 mA cm^{-2} (Fig. 13b). In contrast, aryl-containing ionomers (Sustainion and PiperION) increased the electrode hydrophilicity through the non-covalent interaction, accelerating the HER. This highlights the need to carefully consider ionomer hydrophobicity and compatibility with catalysts before reactions. It is worth mentioning that carbon paper also plays critical roles in modulating electrode hydrophobicity besides the ionomers. The rational design of carbon paper (*e.g.*, increasing PTFE content) enhances the hydrophobicity of the electrode surface.[30] Together, they maintain the entire electrode hydrophobicity. The hydrophobic nature of the electrode facilitates CO_2 mass transport to the three-phase reaction interface while preventing surface flooding.

Moreover, Gong *et al.* modified Ag electrodes with Nafion and other polymers (polyacrylic acid (PAA), polyvinyl alcohol (PVA), and PTFE), observing that their modification could change the contact angle of catalyst surfaces (Fig. 13c). PAA and PVA reduced the hydrophobicity of catalyst surfaces, while Nafion and PTFE enhanced hydrophobicity. Further experimental results demonstrated that hydrophobicity strongly correlated with CO selectivity specifically, increasing with enhanced hydrophobicity of catalyst surfaces (Fig. 13d).[125] They attributed the hydrophobic enhancement of Nafion to its fluorine-rich backbone. Similarly, Wang *et al.* investigated multiple ionomers (Aquivion, Sustainion, PiperION, QAPPT, and Nafion) and found selectivities of C_{2+} and CO positively correlated with hydrophobicity, while formate selectivity decreased (Fig. 13e–g).[126] However, Pention-class ionomers (*e.g.*, D18, D35 and D72) slightly deviated from this trend. This is because their ionic side chains can alter the double-layer structure, affecting C_{2+} selectivity and activity. Bulkier side chains with a lower hydration number form a looser double layer, promoting C–C coupling despite the poorer hydrophobicity. Thus, surface hydrophobicity significantly influences the reaction selectivity, but it is not the sole determinant, and other factors also need to be considered.

4.6 Ionomers modulate structures of interfacial water

The unique structure of ionomers enables some of them to alter interfacial water structures when coated on catalyst surfaces and exposed to electrolytes, thereby modulating the catalytic activity. Interfacial water refers to the transitional water layer between bulk water and another phase, whose properties are significantly altered by interfacial interactions (typically, beyond the first monolayer of water molecules, the subsequent 1–2 molecular layers also exhibit interfacial effects).[127] It possesses unique structural, dynamic, and thermodynamic

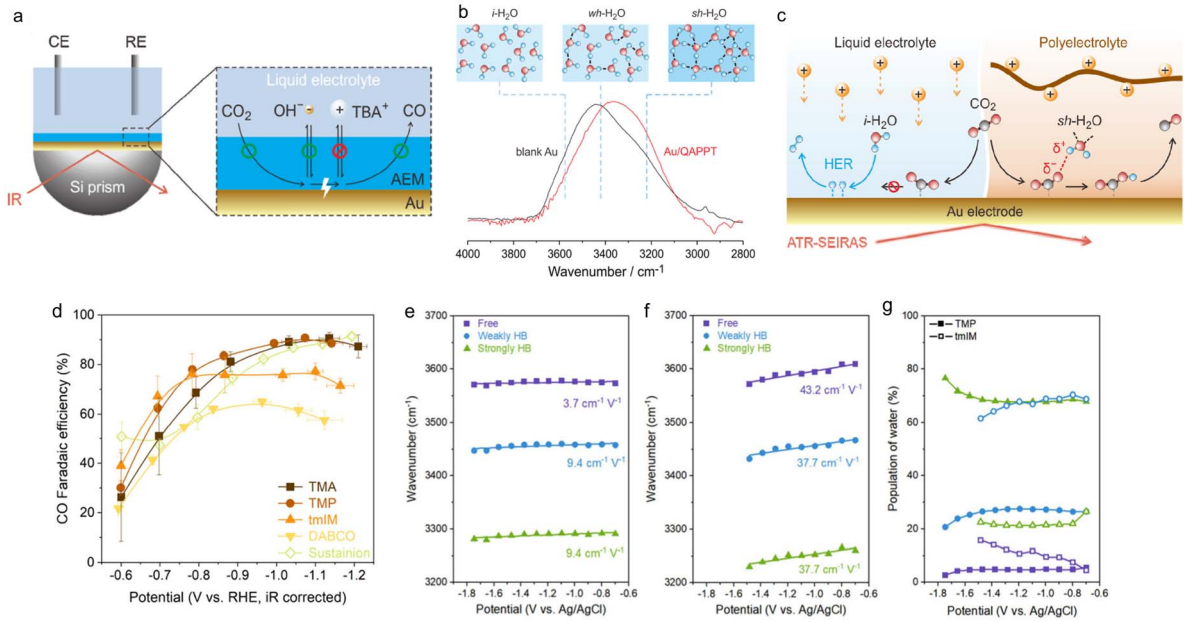

Fig. 14 Ionomers modulate structures of interfacial water at cathodes in the electrocatalytic CO_2RR. (a) Schematic of *in situ* IR and interfacial configuration for the QAPPT-coated Au electrode. (b) The ν(O–H) bands (normalized) recorded at −1.45 V under a CO_2 atmosphere at the interface of blank Au and Au/QAPPT. (c) Mechanism of ionomers altering structures of interfacial water to shift CO_2RR/HER selectivity. Reproduced with permission from ref. 64. Copyright 2024, American Chemical Society. (d) CO selectivity on various QPC-based anion exchange ionomer-modified Ag electrodes. *In situ* IR characterization of interfacial water in CO_2-saturated 0.1 M KCl: wavenumber shifts of water stretching vibrations *versus* potential for (e) TMP-modified and (f) tmIM-modified Ag. (g) Potential-dependent proportions of water structures at TMP/tmIM–Ag interfaces. Reproduced with permission from ref. 94. Copyright 2025, American Chemical Society.

properties. Compared to bulk water, interfacial water exhibits partially broken, distorted, or reconfigured hydrogen-bonded networks, with increased or decreased ordering, and highly oriented molecular alignment. When an ionomer is introduced onto the catalyst surface, interfacial water specifically refers to the water at the catalyst–electrolyte and catalyst–ionomer interfaces (spanning about 2–3 water molecular layers), which may partially extend into the ionomer layer (as shown in Fig. 2b).

Zhuang *et al.* recently coated an Au electrode with the QAPPT ionomer and investigated its effect on catalytic activity and structures of interfacial water through combined electrochemical tests and *in situ* IR (Fig. 14a).[64] Experimental results demonstrated that the QAPPT-modified Au electrode significantly enhanced CO selectivity in the electrocatalytic CO_2RR compared to the bare Au (from <15% increasing to 48%). To elucidate the role of QAPPT, they characterized interfacial species *via in situ* IR, where the QAPPT film was deposited on the Au catalyst. The acquired ν(O–H) band of water was deconvoluted into three components, corresponding to the three structures of interfacial water: the isolated water (*i*-H_2O), the weakly hydrogen-bonded water (*wh*-H_2O), and the strongly hydrogen-bonded water (*sh*-H_2O). Results revealed that QAPPT strengthened the hydrogen-bonded network of interfacial water, notably increasing the proportion of sh-H_2O (Fig. 14b). Correlating with other species changes, they proposed that *sh*-H_2O facilitates *COO hydrogenation to *COOH, promoting selective CO formation (Fig. 14c). Similarly, Won *et al.* explored different ionomers to tailor the interfacial microenvironment, particularly water structures.[94] They synthesized six QPC-based anion exchange ionomers with varied ionic groups. CO_2RR tests showed that the selection of ionic groups dramatically altered CO selectivity, with TMP (trimethyl phosphonium) and tmIM (tetramethylimidazole) groups yielding the better and worse performances, respectively (Fig. 14d). *In situ* IR analysis revealed that the QPC-TMP ionomer induced the restructuring of interfacial water, reducing the Stark tuning slope (from 3.7–9.4 cm^{-1} V^{-1} of QPC-tmIM to 37.7–43.2 cm^{-1} V^{-1} of QPC-TMP) (Fig. 14e and f), while increasing the content of strongly hydrogen-bonded water (from ~20% of QPC-tmIM to 70% of QPC-TMP), which suppressed the HER and favored CO_2 reduction (Fig. 14g). These studies confirm that ionomers can fine-tune the reaction microenvironment by engineering structures of interfacial water, and strongly hydrogen-bonded water favors the selective formation of CO in their testing systems.

5. Summary and outlook

Substantial research efforts have demonstrated that ionomers play a crucial role in the electrocatalytic CO_2RR by precisely modulating the interfacial microenvironment to enable efficient and stable operation. Table 3 summarizes typical ionomers reported in the reaction, including their performances and specific modulation roles. Based on systematic analysis, ionomers modulate the microenvironment primarily through the following ways: (1) ionomers enhance CO_2 mass transport at

Table 3 Performances of the electrocatalytic CO_2RR and the corresponding modulation roles with typical ionomers

Ionomers	Performances	Modulation roles	Ref.
PFSA (Nafion)	$j = 1.32$ A cm^{-2}; $FE_{C_2^+} = 91.7\%$	Promote CO_2 transport	20
QAPEEK	$j = 1$ A cm^{-2}; $FE_{C_2H_4} = 42\%$	Promote CO_2 enrichment	77
LSC-PFSA	$j = 0.6$ A cm^{-2}; $FE_{C_2^+} = 89.4\%$	Modulate CO_2/H_2O transport ratios	63
ρPTN-Beim	$j = 1$ A cm^{-2}; $FE_{C_2H_4} = 33.1\%$	Stabilize intermediates *CO	93
Pention D-18	$j = 0.8$ A cm^{-2}; $FE_{C_2^+} = 85.1\%$	Modulate the pH	88
Naf850/Sus/Cu	$j = 0.02$ A cm^{-2}; $FE_{C2^+} = 90\%$	Modulate the pH and enrich CO_2	21
Polystyrene-based ionomer	$j = 0.274$ A cm^{-2}; $FE_{C_2^+} = 82\%$	Enrich K^+	115
Tp-COF	$j = 0.2$ A cm^{-2}; $FE_{C_2^+} = 75\%$	Enrich K^+	117
Aemion$^+$	$j = 0.1$ A cm^{-2}; $FE_{C_2^+} = 80\%$	Enhance the interfacial electric field	36
c-PDDA	$j = 0.2$ A cm^{-2}; $FE_{CO} = 90\%$	Enhance the interfacial electric field	90
Sustainion XA-9	$j = 0.4$ A cm^{-2}; $FE_{propane} = 90\%$	Stabilize the catalyst	85
Nafion	$j = 0.1$ A cm^{-2}; $FE_{CO} = 99\%$	Enhance hydrophobicity	91
QAPPT	$j = 0.006$ A cm^{-2}; $FE_{CO} = 48\%$	Modulate interfacial H_2O	64

catalyst surfaces and enable selective transport based on molecular polarity of gases. Functional groups (*e.g.*, carbonyl, amine, *etc.*) in ionomers elevate the CO_2 concentration, promoting its enrichment at catalyst surfaces. By designing ionomer structures with segregated CO_2/H_2O transport channels, the CO_2/H_2O ratio at catalyst surfaces can be precisely regulated, simultaneously accelerating CO_2 diffusion and preventing electrode flooding. (2) Designing ionomer structures enables selective adsorption and stabilization of specific reaction intermediates (*e.g.*, linearly adsorbed *CO) and facilitates intermediate diffusion. (3) Ionomers regulate the interfacial pH through selective ion transport and repulsion effects. Multiphysics transport simulations can reveal ion concentrations and transport behaviour within ionomers. A rational combination of multilayer ionomers can increase the surface pH and promote CO_2 mass transport. Well-designed ionomers or their functional groups (*e.g.*, sulfonate and carbonyl groups) can enrich K^+, thereby improving reaction selectivity. Cationic ionomers can mimic alkali metal cations by generating an interfacial electric field to stabilize adsorbed $*CO_2$ or reduction intermediates. (4) The binding effect of ionomers can be used to stabilize the catalyst surface and prevent its reconstruction. The amount of ionomer added significantly affects catalyst dispersion and performance. The mixing method of ionomers with catalysts, as well as the solvents used in the prepared ink solution, greatly influence their performances. (5) Different ionomers usually exhibit varying hydrophilicity/hydrophobicity, and their modification to different catalysts gives rise to distinct effects. Therefore, selective pairing is required during ionomer applications to maximize the hydrophobicity of catalyst surfaces. (6) Ionomers can regulate the structure of interfacial water by forming hydrogen bonds with H_2O, promoting CO_2 reduction.

While significant progress has been made in ionomer research, several challenges remain: (1) many ionomers have poor solubility in common solvents (*e.g.*, ethanol, isopropanol), which significantly limits their applicability. Additionally, due to solvent effects, certain solvents like dimethyl sulfoxide may impact reaction selectivity, and thus careful considerations for ionomer solubility are required. (2) Ionomers face some problems in applications, including their swelling during prolonged operation and structural instability under localized high alkalinity and a strong electric field. (3) Constructing an ordered hydrophilic/hydrophobic channel and a well-aligned CO_2/H_2O transport pathway in ionomers remains highly challenging. (4) When using multilayer ionomers, potential challenges include crosslinking between them and dynamic changes at their interface during reactions. (5) While ionomers can enrich K^+, this capability may concurrently induce issues about salt accumulation. (6) Real-time monitoring of ionomer states under operating conditions, directly elucidating their functional mechanisms, and developing techniques to visualize ion/water transport within ionomers are under development. Facing these challenges, we propose the following recommendations and future research directions based on our understanding: (1) develop diverse ionomer–catalyst mixing methods and coating techniques to achieve faster CO_2 mass transport. (2) Drawing inspiration from Guiver's work,[128] explore magnetic field-assisted fabrication of the ordered ionomer structure to create aligned ion/water transport channels. (3) Design ionomers with inert protective groups to prevent degradation of ionic functional groups. (4) Develop K^+-self-sufficient ionomers to inhibit the binding between K^+ and CO_3^{2-} and salt accumulation. (5) Investigate alkali-metal-free CO_2 electroreduction systems using pure water or acidic electrolyte with ionomers, identifying and resolving underlying scientific challenges. (6) Advance multiscale *operando* characterization techniques to study ionomer behaviour and dynamic changes during reactions.

Regarding the rational selection of ionomers in different systems (acidic, alkaline, and neutral), from the perspective of their ion transport properties (including H^+, K^+, OH^-, CO_3^{2-}, and HCO_3^-), Nafion is more suitable for neutral and alkaline systems, because when used in an acidic system it transports H^+ to the catalyst surface, exacerbating the HER. Cationic ionomers, on the other hand, carry cations that can partially block H^+ transport, making them applicable in acidic systems to maintain a high pH at the catalyst surface. When used in alkaline or neutral systems, cationic ionomers can facilitate the transport of CO_3^{2-} and HCO_3^-, alleviating salt accumulation, which is also beneficial. However, cationic ionomers often

exhibit poor solubility in common alcohol–water solvents, making their effective application challenging. Additionally, many cationic ionomers lack sufficient hydrophobicity, which will easily lead to electrode flooding. In low-concentration or pure water/acid systems, ionomers with higher ionic conductivity need to be selected to enhance ion transport. To be applicable under various reaction conditions, ionomers possessing a combination of properties, including high hydrophobicity, high ion conductivity, selective suppression of H^+ transport, good dispersion with catalysts, ability to enrich CO_2, and stabilization of reaction intermediates, are optimized. We firmly believe that through persistent research and explorations, ionomers will ultimately fulfill their pivotal role in precisely modulating the microenvironment of electrocatalytic CO_2 reduction, enabling highly efficient and stable system operation, making tangible contributions toward achieving the goal of carbon neutrality.

Author contributions

S. R. and S. X. conceived the topic and structure of the review. S. R. wrote the original draft of the manuscript. All authors reviewed and revised the original draft.

Conflicts of interest

There are no conflicts to declare.

Data availability

No primary research results, software or code have been included and no new data were generated or analysed as part of this review.

Acknowledgements

This work was supported by the National Key Research and Development Program of the Ministry of Science and Technology (No. 2022YFA1504600), the National Natural Science Foundation of China (No. 22121001, 22022201, U24A20490, U22A20392, and U23A2087), the Fundamental Research Funds for the Central Universities (No. 20720250005 and 20720240123), and the Fujian Provincial Natural Science Foundation of China (No. 2024J011005).

Notes and references

1 G. Wang, J. Chen, Y. Ding, P. Cai, L. Yi, Y. Li, C. Tu, Y. Hou, Z. Wen and L. Dai, *Chem. Soc. Rev.*, 2021, **50**, 4993–5061.
2 L. Li, X. Li, Y. Sun and Y. Xie, *Chem. Soc. Rev.*, 2022, **51**, 1234–1252.
3 S. Xie, W. Ma, X. Wu, H. Zhang, Q. Zhang, Y. Wang and Y. Wang, *Energy Environ. Sci.*, 2021, **14**, 37–89.
4 W. Ma, X. He, W. Wang, S. Xie, Q. Zhang and Y. Wang, *Chem. Soc. Rev.*, 2021, **50**, 12897–12914.
5 P. Y. Shi, Y. Yan, S. Y. Yang, J. J. Hao, M. Wang and T. B. Lu, *Chem. Sci.*, 2025, **16**, 11711–11739.
6 M. Li, H. Wang, W. Luo, P. C. Sherrell, J. Chen and J. Yang, *Adv. Mater.*, 2020, **32**, e2001848.
7 J. Zhang, W. Cai, F. X. Hu, H. Yang and B. Liu, *Chem. Sci.*, 2021, **12**, 6800–6819.
8 Q. Qu, S. Ji, Y. Chen, D. Wang and Y. Li, *Chem. Sci.*, 2021, **12**, 4201–4215.
9 Y. Zhang, Z. Yao, Y. Yang, X. Zhai, F. Zhang, Z. Guo, X. Liu, B. Yang, Y. Liang, G. Ge and X. Jia, *Chem. Sci.*, 2024, **15**, 13160–13172.
10 J. Han, X. Bai, X. Xu, X. Bai, A. Husile, S. Zhang, L. Qi and J. Guan, *Chem. Sci.*, 2024, **15**, 7870–7907.
11 T. Yan, X. Chen, L. Kumari, J. Lin, M. Li, Q. Fan, H. Chi, T. J. Meyer, S. Zhang and X. Ma, *Chem. Rev.*, 2023, **123**, 10530–10583.
12 D. Gao, R. M. Arán-Ais, H. S. Jeon and B. Roldan Cuenya, *Nat. Catal.*, 2019, **2**, 198–210.
13 Y. Cheng, P. Hou, X. Wang and P. Kang, *Acc. Chem. Res.*, 2022, **55**, 231–240.
14 W. Xie, B. Li, L. Liu, H. Li, M. Yue, Q. Niu, S. Liang, X. Shao, H. Lee, J. Y. Lee, M. Shao, Q. Wang, D. O'Hare and H. He, *Chem. Soc. Rev.*, 2025, **54**, 898–959.
15 D. Gao, P. Wei, H. Li, L. Lin, G. Wang and X. Bao, *Acta Phys. -Chim. Sin.*, 2020, **37**, 2009021.
16 R. Xu, S. Liu, M. Yang, G. Yang, Z. Luo, R. Ran, W. Zhou and Z. Shao, *Chem. Sci.*, 2024, **15**, 11166–11187.
17 C. P. O'Brien, R. K. Miao, A. Shayesteh Zeraati, G. Lee, E. H. Sargent and D. Sinton, *Chem. Rev.*, 2024, **124**, 3648–3693.
18 E. W. Lees, B. A. W. Mowbray, F. G. L. Parlane and C. P. Berlinguette, *Nat. Rev. Mater.*, 2021, **7**, 55–64.
19 D. A. Salvatore, C. M. Gabardo, A. Reyes, C. P. O'Brien, S. Holdcroft, P. Pintauro, B. Bahar, M. Hickner, C. Bae, D. Sinton, E. H. Sargent and C. P. Berlinguette, *Nat. Energy*, 2021, **6**, 339–348.
20 F. P. G. de Arquer, C. T. Dinh, A. Ozden, J. Wicks, C. McCallum, A. R. Kirmani, D. H. Nam, C. Gabardo, A. Seifitokaldani, X. Wang, Y. G. C. Li, F. W. Li, J. Edwards, L. J. Richter, S. J. Thorpe, D. Sinton and E. H. Sargent, *Science*, 2020, **367**, 661–666.
21 C. Kim, J. C. Bui, X. Luo, J. K. Cooper, A. Kusoglu, A. Z. Weber and A. T. Bell, *Nat. Energy*, 2021, **6**, 1026–1034.
22 R. E. Vos and M. T. M. Koper, *ACS Catal.*, 2024, **14**, 4432–4440.
23 R. E. Vos, K. E. Kolmeijer, T. S. Jacobs, W. van der Stam, B. M. Weckhuysen and M. T. M. Koper, *ACS Catal.*, 2023, **13**, 8080–8091.
24 S. Ruan, B. Zhang, J. Zou, W. Zhong, X. He, J. Lu, Q. Zhang, Y. Wang and S. Xie, *Chin. J. Catal.*, 2022, **43**, 3161–3169.
25 A. Reyes, R. P. Jansonius, B. A. W. Mowbray, Y. Cao, D. G. Wheeler, J. Chau, D. J. Dvorak and C. P. Berlinguette, *ACS Energy Lett.*, 2020, **5**, 1612–1618.
26 X. Tan, H. Zhu, C. He, Z. Zhuang, K. Sun, C. Zhang and C. Chen, *Chem. Sci.*, 2024, **15**, 4292–4312.
27 H. Li, N. Xiao, Y. Wang, C. Liu, S. Zhang, H. Zhang, J. Bai, J. Xiao, C. Li, Z. Guo, S. Zhao and J. Qiu, *J. Mater. Chem. A*, 2020, **8**, 1779–1786.

28 Y. Pan, R. Lin, Y. Chen, S. Liu, W. Zhu, X. Cao, W. Chen, K. Wu, W. C. Cheong, Y. Wang, L. Zheng, J. Luo, Y. Lin, Y. Liu, C. Liu, J. Li, Q. Lu, X. Chen, D. Wang, Q. Peng, C. Chen and Y. Li, *J. Am. Chem. Soc.*, 2018, **140**, 4218–4221.
29 Z. Qin, H. Zhuang, D. Song, G. Zhang, H. Gao, X. Du, M. Jiang, P. Zhang and J. Gong, *Chem. Sci.*, 2025, **16**, 5872–5879.
30 T. N. Nguyen and C. T. Dinh, *Chem. Soc. Rev.*, 2020, **49**, 7488–7504.
31 Y. Rong, J. Sang, L. Che, D. Gao and G. Wang, *Acta Phys. -Chim. Sin.*, 2023, **39**, 2212027.
32 Y. Chae, H. Kim, D. K. Lee, U. Lee and D. H. Won, *Nano Energy*, 2024, **130**, 110134.
33 H. Deng, Z. Chen and Y. Wang, *ChemSusChem*, 2025, **18**, e202401728.
34 J. J. Lv, R. Yin, L. Zhou, J. Li, R. Kikas, T. Xu, Z. J. Wang, H. Jin, X. Wang and S. Wang, *Angew. Chem., Int. Ed.*, 2022, **61**, e202207252.
35 J. C. Bui, C. Kim, A. J. King, O. Romiluyi, A. Kusoglu, A. Z. Weber and A. T. Bell, *Acc. Chem. Res.*, 2022, **55**, 484–494.
36 M. Fan, J. E. Huang, R. K. Miao, Y. Mao, P. Ou, F. Li, X.-Y. Li, Y. Cao, Z. Zhang, J. Zhang, Y. Yan, A. Ozden, W. Ni, Y. Wang, Y. Zhao, Z. Chen, B. Khatir, C. P. O'Brien, Y. Xu, Y. C. Xiao, G. I. N. Waterhouse, K. Golovin, Z. Wang, E. H. Sargent and D. Sinton, *Nat. Catal.*, 2023, **6**, 763–772.
37 D. Li, E. J. Park, W. Zhu, Q. Shi, Y. Zhou, H. Tian, Y. Lin, A. Serov, B. Zulevi, E. D. Baca, C. Fujimoto, H. T. Chung and Y. S. Kim, *Nat. Energy*, 2020, **5**, 378–385.
38 J. Wang, Y. Zhao, B. P. Setzler, S. Rojas-Carbonell, C. Ben Yehuda, A. Amel, M. Page, L. Wang, K. Hu, L. Shi, S. Gottesfeld, B. Xu and Y. Yan, *Nat. Energy*, 2019, **4**, 392–398.
39 S. Maurya, S. Noh, I. Matanovic, E. J. Park, C. Narvaez Villarrubia, U. Martinez, J. Han, C. Bae and Y. S. Kim, *Energy Environ. Sci.*, 2018, **11**, 3283–3291.
40 F. Chen, L. Guo, D. Long, S. Luo, Y. Song, M. Wang, L. Li, S. Chen and Z. Wei, *J. Am. Chem. Soc.*, 2024, **146**, 30388–30396.
41 R. B. Kutz, Q. Chen, H. Yang, S. D. Sajjad, Z. Liu and I. R. Masel, *Energy Technol.*, 2017, **5**, 929–936.
42 S. Lu, Y. Wang, H. Xiang, H. Lei, B. B. Xu, L. Xing, E. H. Yu and T. X. Liu, *J. Energy Storage*, 2022, **52**, 104764.
43 X. Nie, M. R. Esopi, M. J. Janik and A. Asthagiri, *Angew. Chem., Int. Ed.*, 2013, **52**, 2459–2462.
44 Z. S. Zhu, S. Zhong, C. Cheng, H. Zhou, H. Sun, X. Duan and S. Wang, *Chem. Rev.*, 2024, **124**, 11348–11434.
45 C. Chen, H. Jin, P. Wang, X. Sun, M. Jaroniec, Y. Zheng and S. Z. Qiao, *Chem. Soc. Rev.*, 2024, **53**, 2022–2055.
46 X. Yang, W. Song, T. Zhang, Z. Huang, J. Zhang, J. Ding and W. Hu, *Adv. Energy Mater.*, 2023, **13**, 2301737.
47 A. B. Grommet, M. Feller and R. Klajn, *Nat. Nanotechnol.*, 2020, **15**, 256–271.
48 C. Xie, Z. Niu, D. Kim, M. Li and P. Yang, *Chem. Rev.*, 2020, **120**, 1184–1249.
49 T. L. Soucy, W. S. Dean, J. Zhou, K. E. Rivera Cruz and C. C. L. McCrory, *Acc. Chem. Res.*, 2022, **55**, 252–261.
50 Z. Wang, Y. Li, C. Wu and S. C. E. Tsang, *Joule*, 2022, **6**, 1798–1825.
51 X. Chen, C. Chen, Y. Wang, Z. Pan, J. Chen, Y. Xu, L. Zhu, T. Song, R. Li, L. Chen and J. Lu, *Chem. Eng. J.*, 2024, **482**, 148944.
52 J. Gu, S. Liu, W. Ni, W. Ren, S. Haussener and X. Hu, *Nat. Catal.*, 2022, **5**, 268–276.
53 Z. Ma, Z. Yang, W. Lai, Q. Wang, Y. Qiao, H. Tao, C. Lian, M. Liu, C. Ma, A. Pan and H. Huang, *Nat. Commun.*, 2022, **13**, 7596.
54 D. H. Nam, P. De Luna, A. Rosas-Hernandez, A. Thevenon, F. W. Li, T. Agapie, J. C. Peters, O. Shekhah, M. Eddaoudi and E. H. Sargent, *Nat. Mater.*, 2020, **19**, 266–276.
55 P. Wei, D. Gao, T. Liu, H. Li, J. Sang, C. Wang, R. Cai, G. Wang and X. Bao, *Nat. Nanotechnol.*, 2023, **18**, 299–306.
56 M. Konig, J. Vaes, E. Klemm and D. Pant, *iScience*, 2019, **19**, 135–160.
57 W. Fang, W. Guo, R. Lu, Y. Yan, X. Liu, D. Wu, F. M. Li, Y. Zhou, C. He, C. Xia, H. Niu, S. Wang, Y. Liu, Y. Mao, C. Zhang, B. You, Y. Pang, L. Duan, X. Yang, F. Song, T. Zhai, G. Wang, X. Guo, B. Tan, T. Yao, Z. Wang and B. Y. Xia, *Nature*, 2024, **626**, 86–91.
58 Z. C. Liu, H. Z. Yang, R. Kutz and R. I. Masel, *J. Electrochem. Soc.*, 2018, **165**, J3371–J3377.
59 B. Endrődi, E. Kecsenovity, A. Samu, T. Halmágyi, S. Rojas-Carbonell, L. Wang, Y. Yan and C. Janáky, *Energy Environ. Sci.*, 2020, **13**, 4098–4105.
60 D. M. Weekes, D. A. Salvatore, A. Reyes, A. Huang and C. P. Berlinguette, *Acc. Chem. Res.*, 2018, **51**, 910–918.
61 T. Tang, X. Bai, Z. Wang and J. Guan, *Chem. Sci.*, 2024, **15**, 5082–5112.
62 K. N. Kolding, K. Torbensen and A. Rosas-Hernandez, *Chem. Sci.*, 2025, **16**, 6136–6159.
63 J. Sun, B. Wu, Z. Wang, H. Guo, G. Yan, H. Duan, G. Li, Y. Wang and J. Wang, *Energy Environ. Sci.*, 2025, **18**, 1027–1037.
64 Z. Mi, T. Wang, L. Xiao, G. Wang and L. Zhuang, *J. Am. Chem. Soc.*, 2024, **146**, 17377–17383.
65 S. Li, G. Wu, J. Mao, A. Chen, X. Liu, J. Zeng, Y. Wei, J. Wang, H. Zhu, J. Xia, X. Wang, G. Li, Y. Song, X. Dong, W. Wei and W. Chen, *Angew. Chem., Int. Ed.*, 2024, e202407612.
66 C. Chen, X. Zhu, X. Wen, Y. Zhou, L. Zhou, H. Li, L. Tao, Q. Li, S. Du, T. Liu, D. Yan, C. Xie, Y. Zou, Y. Wang, R. Chen, J. Huo, Y. Li, J. Cheng, H. Su, X. Zhao, W. Cheng, Q. Liu, H. Lin, J. Luo, J. Chen, M. Dong, K. Cheng, C. Li and S. Wang, *Nat. Chem.*, 2020, **12**, 717–724.
67 C. Lv, L. Zhong, H. Liu, Z. Fang, C. Yan, M. Chen, Y. Kong, C. Lee, D. Liu, S. Li, J. Liu, L. Song, G. Chen, Q. Yan and G. Yu, *Nat. Sustain.*, 2021, **4**, 868–876.
68 W. Zhong, W. Huang, S. Ruan, Q. Zhang, Y. Wang and S. Xie, *Chem.–Eur. J.*, 2023, **29**, e202203228.
69 C. T. Dinh, T. Burdyny, M. G. Kibria, A. Seifitokaldani, C. M. Gabardo, F. P. G. de Arquer, A. Kiani, J. P. Edwards, P. De Luna, O. S. Bushuyev, C. Q. Zou, R. Quintero-Bermudez, Y. J. Pang, D. Sinton and E. H. Sargent, *Science*, 2018, **360**, 783–787.

70 K. V. Petrov, C. I. Koopman, S. Subramanian, M. T. M. Koper, T. Burdyny and D. A. Vermaas, *Nat. Energy*, 2024, **9**, 932–938.
71 X. She, L. Zhai, Y. Wang, P. Xiong, M. M.-J. Li, T.-S. Wu, M. C. Wong, X. Guo, Z. Xu, H. Li, H. Xu, Y. Zhu, S. C. E. Tsang and S. P. Lau, *Nat. Energy*, 2024, **9**, 81–91.
72 Z. Yan, J. L. Hitt, Z. Zeng, M. A. Hickner and T. E. Mallouk, *Nat. Chem.*, 2021, **13**, 33–40.
73 C. Xia, P. Zhu, Q. Jiang, Y. Pan, W. T. Liang, E. Stavitski, H. N. Alshareef and H. T. Wang, *Nat. Energy*, 2019, **4**, 776–785.
74 G. Wen, B. Ren, X. Wang, D. Luo, H. Dou, Y. Zheng, R. Gao, J. Gostick, A. Yu and Z. Chen, *Nat. Energy*, 2022, **7**, 978–988.
75 A. Kusoglu and A. Z. Weber, *Chem. Rev.*, 2017, **117**, 987–1104.
76 A. Ozden, F. W. Li, F. P. G. de Arquer, A. Rosas-Hernandez, A. Thevenon, Y. H. Wang, S. F. Hung, X. Wang, B. Chen, J. Li, J. Wicks, M. C. Luo, Z. Y. Wang, T. Agapie, J. C. Peters, E. H. Sargent and D. Sinton, *ACS Energy Lett.*, 2020, **5**, 2811–2818.
77 W. Li, Z. Yin, Z. Gao, G. Wang, Z. Li, F. Wei, X. Wei, H. Peng, X. Hu, L. Xiao, J. Lu and L. Zhuang, *Nat. Energy*, 2022, **7**, 835–843.
78 Y. Xu, R. K. Miao, J. P. Edwards, S. Liu, C. P. O'Brien, C. M. Gabardo, M. Fan, J. E. Huang, A. Robb, E. H. Sargent and D. Sinton, *Joule*, 2022, **6**, 1333–1343.
79 R. Xue, S. Yuan, R. Wang, T. Bi, G. Zhang, H. Li, J. Yin, L. Luo, S. Shen, X. Yan and J. Zhang, *J. Energy Chem.*, 2025, **108**, 390–399.
80 D. R. Lide, *CRC Handbook of Chemistry and Physics*, 85th edn, CRC, 2004.
81 H. Peng, Q. Li, M. Hu, L. Xiao, J. Lu and L. Zhuang, *J. Power Sources*, 2018, **390**, 165–167.
82 Z. Lu, M. Lugo, M. H. Santare, A. M. Karlsson, F. C. Busby and P. Walsh, *J. Power Sources*, 2012, **214**, 130–136.
83 H. Z. Yang, J. J. Kaczur, S. D. Sajjad and R. I. Masel, *J. CO_2 Util.*, 2017, **20**, 208–217.
84 M. Rashid, S. K. Nabil, M. A. Adnan, K. Kannimuthu and M. G. Kibria, *Adv. Energy Mater.*, 2024, **14**, 2400570.
85 M. Esmaeilirad, Z. Jiang, A. M. Harzandi, A. Kondori, M. Tamadoni Saray, C. U. Segre, R. Shahbazian-Yassar, A. M. Rappe and M. Asadi, *Nat. Energy*, 2023, **8**, 891–900.
86 Y. I. Song, B. Yoon, C. Lee, D. Kim, M. H. Han, H. Han, W. H. Lee, D. H. Won, J. K. Kim, H. S. Jeon and J. H. Koh, *Adv. Sci.*, 2024, **11**, e2406281.
87 Y. E. Kim, W. Lee, Y. N. Ko, J. E. Park, D. Tan, J. Hong, Y. E. Jeon, J. Oh and K. T. Park, *ACS Sustainable Chem. Eng.*, 2022, **10**, 11710–11718.
88 Y. Zhao, X. Zu, R. Chen, X. Li, Y. Jiang, Z. Wang, S. Wang, Y. Wu, Y. Sun and Y. Xie, *J. Am. Chem. Soc.*, 2022, **144**, 10446–10454.
89 M. Zhuansun, Y. Liu, R. Lu, F. Zeng, Z. Xu, Y. Wang, Y. Yang, Z. Wang, G. Zheng and Y. Wang, *Angew. Chem., Int. Ed.*, 2023, **62**, e202309875.
90 H. G. Qin, Y. F. Du, Y. Y. Bai, F. Z. Li, X. Yue, H. Wang, J. Z. Peng and J. Gu, *Nat. Commun.*, 2023, **14**, 5640.
91 C. Yu, T. Lei, L. Xu, C. Jin, J. Yi, S. Liu, S. Lin, Y. Yang, H. Song, K. Wang, H. Fan, C. Zheng, X. Zhang and X. Gao, *J. Mater. Chem. A*, 2024, **12**, 17181–17192.
92 Z. Yin, H. Peng, X. Wei, H. Zhou, J. Gong, M. Huai, L. Xiao, G. Wang, J. Lu and L. Zhuang, *Energy Environ. Sci.*, 2019, **12**, 2455–2462.
93 L. Xue, Z. Gao, T. Ning, W. Li, J. Li, J. Yin, L. Xiao, G. Wang and L. Zhuang, *Angew. Chem., Int. Ed.*, 2023, **62**, e202309519.
94 W. Jung, S.-H. Shin, S. Park, Y. Chae, U. Lee, H. J. Cho, S. Kim, Y. J. Hwang, J. Y. Lee and D. H. Won, *ACS Energy Lett.*, 2025, **10**, 620–628.
95 J. T. A. Zawodzinski, M. Neeman, L. O. Sillerud and S. Gottesfeld, *J. Phys. Chem.*, 1991, **95**, 6040–6044.
96 M. E. Tuckerman, D. Marx and M. Parrinello, *Nature*, 2002, **417**, 925–929.
97 J. Kamcev and B. D. Freeman, *Annu. Rev. Chem. Biomol. Eng.*, 2016, **7**, 111–133.
98 S. Garg, C. A. Giron Rodriguez, T. E. Rufford, J. R. Varcoe and B. Seger, *Energy Environ. Sci.*, 2022, **15**, 4440–4469.
99 P. Papangelakis, R. K. Miao, R. Lu, H. Liu, X. Wang, A. Ozden, S. Liu, N. Sun, C. P. O'Brien, Y. Hu, M. Shakouri, Q. Xiao, M. Li, B. Khatir, J. E. Huang, Y. Wang, Y. C. Xiao, F. Li, A. S. Zeraati, Q. Zhang, P. Liu, K. Golovin, J. Y. Howe, H. Liang, Z. Wang, J. Li, E. H. Sargent and D. Sinton, *Nat. Energy*, 2024, **9**, 1011–1020.
100 J. Wang, T. Cheng, A. Q. Fenwick, T. N. Baroud, A. Rosas-Hernandez, J. H. Ko, Q. Gan, W. A. Goddard, III and R. H. Grubbs, *J. Am. Chem. Soc.*, 2021, **143**, 2857–2865.
101 X.-Q. Li, G.-Y. Duan, J.-W. Chen, L.-J. Han, S.-J. Zhang and B.-H. Xu, *Appl. Catal. B Environ.*, 2021, **297**, 120471.
102 X. Lu, T. Gankhuyag, K. Obata, Y. Yu and K. Takanabe, *Chem Catal.*, 2024, **4**, 101030.
103 A. Ozden, Y. Wang, F. Li, M. Luo, J. Sisler, A. Thevenon, A. Rosas-Hernández, T. Burdyny, Y. Lum, H. Yadegari, T. Agapie, J. C. Peters, E. H. Sargent and D. Sinton, *Joule*, 2021, **5**, 706–719.
104 J. Yi, E. M. You, R. Hu, D. Y. Wu, G. K. Liu, Z. L. Yang, H. Zhang, Y. Gu, Y. H. Wang, X. Wang, H. Ma, Y. Yang, J. Y. Liu, F. R. Fan, C. Zhan, J. H. Tian, Y. Qiao, H. Wang, S. H. Luo, Z. D. Meng, B. W. Mao, J. F. Li, B. Ren, J. Aizpurua, V. A. Apkarian, P. N. Bartlett, J. Baumberg, S. E. J. Bell, A. G. Brolo, L. E. Brus, J. Choo, L. Cui, V. Deckert, K. F. Domke, Z. C. Dong, S. Duan, K. Faulds, R. Frontiera, N. Halas, C. Haynes, T. Itoh, J. Kneipp, K. Kneipp, E. C. Le Ru, Z. P. Li, X. Y. Ling, J. Lipkowski, L. M. Liz-Marzan, J. M. Nam, S. Nie, P. Nordlander, Y. Ozaki, R. Panneerselvam, J. Popp, A. E. Russell, S. Schlucker, Y. Tian, L. Tong, H. Xu, Y. Xu, L. Yang, J. Yao, J. Zhang, Y. Zhang, Y. Zhang, B. Zhao, R. Zenobi, G. C. Schatz, D. Graham and Z. Q. Tian, *Chem. Soc. Rev.*, 2025, **54**, 1453–1551.
105 J. Kozuch, K. Ataka and J. Heberle, *Nat. Rev. Methods Primers*, 2023, **3**, 70.

106 J. Park, Y. Chae, C. Lee, G. Kwon, W. H. Lee, H. S. Jeon, J. Cho, D. H. Won and J. H. Koh, *ACS Catal.*, 2025, **15**, 12222–12230.
107 Y. Chen, J. A. Wrubel, A. E. Vise, F. Intia, S. Harshberger, E. Klein, W. A. Smith, Z. Ma, T. G. Deutsch and K. C. Neyerlin, *Chem Catal.*, 2022, **2**, 400–421.
108 M. L. J. Peerlings, M. E. T. Vink-van Ittersum, J. W. de Rijk, P. E. de Jongh and P. Ngene, *ACS Catal.*, 2025, **15**, 9695–9705.
109 W. Ren, A. Xu, K. Chan and X. Hu, *Angew. Chem., Int. Ed.*, 2022, **61**, e202214173.
110 B. Pan, Y. Wang and Y. Li, *Chem Catal.*, 2022, **2**, 1267–1276.
111 J. Resasco, L. D. Chen, E. Clark, C. Tsai, C. Hahn, T. F. Jaramillo, K. Chan and A. T. Bell, *J. Am. Chem. Soc.*, 2017, **139**, 11277–11287.
112 X. Yang, H. Ding, S. Li, S. Zheng, J. F. Li and F. Pan, *J. Am. Chem. Soc.*, 2024, **146**, 5532–5542.
113 B. Endrodi, A. Samu, E. Kecsenovity, T. Halmagyi, D. Sebok and C. Janaky, *Nat. Energy*, 2021, **6**, 439–448.
114 M. C. O. Monteiro, F. Dattila, B. Hagedoorn, R. García-Muelas, N. López and M. T. M. Koper, *Nat. Catal.*, 2021, **4**, 654–662.
115 G. P. Heim, M. A. Bruening, C. B. Musgrave, W. A. Goddard, J. C. Peters and T. Agapie, *Joule*, 2024, **8**, 1312–1321.
116 Z. Zhu, Y. Zhu, Z. Ren, D. Liu, F. Yue, D. Sheng, P. Shao, X. Huang, X. Feng, A. X. Yin, J. Xie and B. Wang, *J. Am. Chem. Soc.*, 2024, **146**, 1572–1579.
117 Y. Zhao, L. Hao, A. Ozden, S. Liu, R. K. Miao, P. Ou, T. Alkayyali, S. Zhang, J. Ning, Y. Liang, Y. Xu, M. Fan, Y. Chen, J. E. Huang, K. Xie, J. Zhang, C. P. O'Brien, F. Li, E. H. Sargent and D. Sinton, *Nat. Synth.*, 2023, **2**, 403–412.
118 Z.-M. Zhang, T. Wang, Y.-C. Cai, X.-Y. Li, J.-Y. Ye, Y. Zhou, N. Tian, Z.-Y. Zhou and S.-G. Sun, *Nat. Catal.*, 2024, **7**, 807–817.
119 J. Fan, B. Pan, J. Wu, C. Shao, Z. Wen, Y. Yan, Y. Wang and Y. Li, *Angew. Chem., Int. Ed.*, 2024, **63**, e202317828.
120 X. Zhao, H. Xie, B. Deng, L. Wang, Y. Li and F. Dong, *Chem. Commun.*, 2024, **60**, 542–545.
121 J. A. Abarca, L. Warmuth, A. Rieder, A. Dutta, S. Vesztergom, P. Broekmann, A. Irabien and G. Díaz-Sainz, *ACS Catal.*, 2025, **15**, 8753–8767.
122 X. Du, P. Zhang, G. Zhang, H. Gao, L. Zhang, M. Zhang, T. Wang and J. Gong, *Natl. Sci. Rev.*, 2024, **11**, nwad149.
123 B. A. W. Mowbray, D. J. Dvorak, N. Taherimakhsousi and C. P. Berlinguette, *Energy Fuels*, 2021, **35**, 19178–19184.
124 E. W. Lees, B. A. W. Mowbray, D. A. Salvatore, G. L. Simpson, D. J. Dvorak, S. X. Ren, J. Chau, K. L. Milton and C. P. Berlinguette, *J. Mater. Chem. A*, 2020, **8**, 19493–19501.
125 Q. Chang, G. Zhang, J. Chen, X. Du, C. Wang, Y. Cai, Y. Du, P. Zhang, T. Wang and J. Gong, *J. Energy Chem.*, 2025, **108**, 373–380.
126 F. Zeng, H. Deng, M. Zhuansun, W. Teng and Y. Wang, *J. Mater. Chem. A*, 2024, **12**, 20990–20998.
127 Y. H. Wang, S. Zheng, W. M. Yang, R. Y. Zhou, Q. F. He, P. Radjenovic, J. C. Dong, S. Li, J. Zheng, Z. L. Yang, G. Attard, F. Pan, Z. Q. Tian and J. F. Li, *Nature*, 2021, **600**, 81–85.
128 X. Liu, N. Xie, J. Xue, M. Li, C. Zheng, J. Zhang, Y. Qin, Y. Yin, D. R. Dekel and M. D. Guiver, *Nat. Energy*, 2022, **7**, 329–339.